



1 **Bayesian Inference and Predictive Performance of Soil Respiration Models in the Presence**
2 **of Model Discrepancy**

3

4 Ahmed S. Elshall^{1,2}, Ming Ye^{3,*}, Guo-Yue Niu^{4,5} and Greg A. Barron-Gafford^{4,6}

5

6 ¹Department of Geosciences, University of Hawaii Manoa, Honolulu, Hawaii, USA

7 ²Water Resources Research Center, University of Hawaii Manoa, Honolulu, Hawaii, USA

8 ³Department of Earth, Ocean, and Atmospheric Science, Florida State University, Tallahassee,
9 Florida

10 ⁴Biosphere 2, University of Arizona, Tucson, Arizona

11 ⁵Department of Hydrology and Water Resources, University of Arizona, Tucson, Arizona

12 ⁶School of Geography and Development, University of Arizona, Tucson, Arizona

13

14

15 *Corresponding Author: Ming Ye, Telephone: (850) 644-4587, Email: mye@fsu.edu

16

17

18

19

20

21

22

23

24

25

26

27

28

29

30

31

32

33

34

35

36

37

38

39

40

41

42

43

44

45

46



47 **Key Points**

48

49 (1) Bayesian inference and prediction are useful to evaluate multiple soil respiration models
50 with different levels of complexity.

51 (2) Data models used in Bayesian inference have substantial impacts on model parameter
52 distributions and subsequently model predictions.

53 (3) Using exponential power distribution and considering heteroscedasticity in data models
54 improves Bayesian inference and prediction.

55

56

57

58

59

60

61

62

63

64

65

66

67 Keywords: Soil respiration, Bayesian, likelihood function, data model, autocorrelation,
68 heteroscedasticity, skew exponential power distribution, cross-validation, relative model score

69

70



71 **Abstract**

72 Bayesian inference of microbial soil respiration models is often based on the assumptions that the
73 residuals are independent (i.e. no temporal or spatial correlation), identically distributed (i.e.
74 Gaussian noise) and with constant variance (i.e. homoscedastic). In the presence of model
75 discrepancy, since no model is perfect, this study shows that these assumptions are generally
76 invalid in soil respiration modeling such that residuals have high temporal correlation, an
77 increasing variance with increasing magnitude of CO₂ efflux, and non-Gaussian distribution.
78 Relaxing these three assumptions stepwise results in eight data models. Data models are the basis
79 of formulating likelihood functions of Bayesian inference. This study presents a systematic and
80 comprehensive investigation of the impacts data model selection on Bayesian inference and
81 predictive performance. We use three mechanistic soil respiration models with different levels of
82 model fidelity (i.e. model discrepancy) with respect to number of carbon pools and explicit
83 representations of soil moisture controls on carbon degradation, and accordingly have different
84 levels of model complexity with respect to the number of model parameters. The study shows data
85 models have substantial impacts on Bayesian inference and predictive performance of the soil
86 respiration models such that: (i) the level of complexity of the best model is generally justified by
87 the cross-validation results for different data models; (ii) not accounting for heteroscedasticity and
88 autocorrelation might not necessarily result in biased parameter estimates or predictions, but will
89 definitely underestimate uncertainty; (iii) using a non-Gaussian data model improves the parameter
90 estimates and the predictive performance; and (iv) separate accounting for autocorrelation or joint
91 inversion of correlation and heteroscedasticity can be problematic and requires special treatment.
92 Although the conclusions of this study are empirical, the analysis may provide insights for
93 selecting appropriate data models for soil respiration models.



94 1 Introduction

95 Developing accurate soil respiration models is important for realistic projection of global
96 carbon [C] cycle, as global soils store 2,300Pg carbon, an amount more than 3 times that of the
97 atmosphere (Schmidt et al., 2011) and release 60–75 Pg C/yr, about 7 times more CO₂ to the
98 atmosphere than all human-caused emissions (Le Quéré et al., 2014). The major work on soil
99 respiration modeling has been focused on advancing knowledge about model inputs and
100 calibration data (e.g. Janssens et al., 2003; Peters et al., 2007; Scott et al., 2009; Barron-Gafford et
101 al., 2011; Hilton et al., 2014) and on developing more advanced models for better representing
102 soil microbial processes (e.g. Schimel and Weintraub, 2003; Allison et al., 2010; Davidson et al.,
103 2011; Wieder et al., 2013, 2015; Xu et al., 2014; Zhang et al., 2014) . Integration of data and
104 models is indispensable for improving predictability of the terrestrial carbon cycle, and statistical
105 modeling is a vital tool for the model-data integration (Luo et al., 2011, 2014; Wieder et al., 2015).
106 In addition, use of state-of-the-art statistical methods is necessary to accurately quantify
107 uncertainty in parameters and structures of soil respiration models for improvement and practical
108 uses of the models (Katz et al., 2013). Statistical modeling always requires adequately
109 characterizing residuals, i.e., the difference between data and corresponding model simulations.
110 While a large number of data models have been used, to our knowledge, comprehensive and
111 systematic evaluation of data models for soil respiration models has not been reported in literature.

112 The goal of this study is to evaluate the impacts of data models on Bayesian inference and
113 predictive performance of three mechanistic soil respiration models, and use these findings to
114 make broader recommendations. The three models were developed by Zhang et al. (2014) to
115 simulate the Birch effect (the peak soil microbial respiration pulses in response to episodic rainfall
116 pulses) at a site scale and a short temporal scale, which are important for gaining mechanistic



117 understanding of CO₂ efflux production (Högberg and Read, 2006; Vargas et al., 2011). Zhang et
118 al. (2014) developed a total five models, including an existing four-carbon pool model and four
119 new models with additional carbon pools and/or explicit representations of soil moisture controls
120 on carbon degradation and microbial uptake rates. The models Zhang et al. (2014) were calibrated,
121 and Bayesian model selection was used to select and the best model. However, this effort was
122 based on a single data model. It is unknown whether the best model still remains the best (in terms
123 of reproducing the both calibration data and the cross-validation data) if a different data model is
124 used. In addition, since predictive performance of the models was not evaluated in Zhang et al.
125 (2014), it is unknown whether the best model will give the best predictions. These two questions
126 are addressed in this study by considering eight data models and by evaluating predictive
127 performance in a manner of cross-validation. The top two models (also the two most high fidelity
128 models) ranked by Zhang et al. (2014) are considered in this study, and the worst model (also the
129 low fidelity model) is also considered in this study for comparison. Model fidelity refers to the
130 degree of realism of representing our scientific knowledge with respect to the real world system.
131 That is model with less discrepancy. Conducting Bayesian inference and evaluating predictive
132 performance for the three models with different degrees of fidelity provides more insights than for
133 a single model.

134 Bayesian inference in general uses the Bayes' theorem to update the distributions of model
135 parameters to posterior parameter distributions given a likelihood function. The mathematical
136 formulation of the (formal and informal) likelihood function requires a probabilistic data model
137 that however is intrinsically unknown due to unknown errors in all model components such as
138 observation data, model structures, parameters, and driving forces. Bayesian inference of soil
139 respiration models often adopts the assumption of independent, normally distributed and



140 homoscedastic residuals (e.g. Ahrens et al., 2014; Barr et al., 2013; Hararuk et al., 2014;
141 Hashimoto et al., 2011; Klemedtsson et al., 2008; Raich et al., 2002; Ren et al., 2013; Ricciuto et
142 al., 2011; Richardson and Hollinger, 2005; Steinacher and Joos, 2016; Tucker et al., 2014; Tuomi
143 et al., 2008; Xu et al., 2006; Yeluripati et al., 2009; Zhang et al., 2014; Zhou et al., 2010). These
144 assumptions are conveniently adopted since the requirement of using an unknown probability
145 model in Bayesian statistics is called “a basic dilemma” by Box and Tiao (1992). Postulating the
146 data models is always based on assumptions about residual statistics, and the most widely used
147 assumptions are paired as follows: (i) independent vs. correlated residuals, (ii) homoscedastic vs.
148 heteroscedastic residuals, and (iii) Gaussian vs. non-Gaussian residuals. There are many
149 diagnostics available to assess these choices (a number of them is used in this paper). However,
150 few studies have focused on investigating appropriateness of the assumptions for soil respiration
151 modeling by relaxing the independent residuals assumption (Chevallier and O’Dell, 2013; Ricciuto
152 et al., 2011) and the Gaussian residuals assumption (Ricciuto et al., 2011; Van Wijk et al., 2008).

153 This study evaluates the above assumptions by considering eight data models which relaxes
154 these three assumptions stepwise as shown in Section 2. For example, combining the assumptions
155 of independent, homoscedastic, and Gaussian residuals leads to the standard least squares data
156 model. This model is the simplest one among the eight data models, since it requires only one
157 parameter, i.e., the constant variance of the Gaussian distribution. Note that there is a difference
158 between the physical model parameters and data model parameters. They technically can be
159 estimated together, but one arises from assumptions about process, and the other assumptions
160 about the data models. Relaxing the homoscedastic assumption to heteroscedastic gives the
161 weighted least squares data model. It is more complex, because it requires multiple variances for
162 multiple data. Whenever one or combinations of the three assumptions (independence,



163 homoscedasticity, and normality) are relaxed, the resulting data models become more complex and
164 require more parameters. This systematic way of formulating data models is similar to that of
165 Smith et al. (2010b, 2015), and it is necessary to evaluate appropriateness of the three basic
166 assumptions and their impacts on Bayesian inference.

167 The assumptions of heteroscedastic, correlated, and non-Gaussian residuals are accounted for
168 using the method of Schoups and Vrugt (2010) in the following procedure: (i) the correlation is
169 removed from the residuals by using an autoregressive model; (ii) the resulting residuals are
170 normalized by a linear model of variance; and (iii) the normalized residuals are characterized by
171 using the skew exponential power distribution. The data model parameters (i.e., coefficients of the
172 autoregressive model, the linear variance model, and the skew exponential power distribution) are
173 not specified by users, but estimated together with physical model parameters during the Bayesian
174 inference. The skew exponential power distribution is general in that by adjusting the values of its
175 kurtosis and skewness parameters the distribution can produce other distributions such as the
176 Laplace distribution used by (Van Wijk et al., 2008) and (Ricciuto et al., 2011), and other
177 distributions given by using different kurtosis parameters of an exponential model (Tang and
178 Zhuang, 2009). It is worth pointing out that there exist other methods to account for the three
179 assumptions. Evin et al. (2013) suggested accounting for residual heteroscedasticity before
180 accounting for residual autocorrelation. Lu et al. (2013) developed an iterative two-stage procedure
181 to separately estimate physical model parameters and data model parameters. Evin et al. (2014)
182 developed a similar procedure to first estimate model parameters and then estimate
183 heteroscedasticity and autocorrelation parameters. While this study uses the method of Schoups
184 and Vrugt (2010), exploring other methods is warranted in future studies.



185 After investigating the impacts of the data models on Bayesian inference, this study evaluates
186 the impacts of the data models on predictive performance of the three soil respiration models.
187 Using random samples generated during the Bayesian inference, a prediction ensemble is produced
188 for each soil respiration model. The ensemble is used to evaluate predictive performance of the
189 models in a stochastic sense by estimating to what extent the models can predict future events. The
190 evaluation in this study is done in a cross-validation manner to split a dataset of CO₂ efflux into
191 two parts for Bayesian inference and cross-validation, respectively. The evaluation of predictive
192 performance is important because different data models may give different parameter distributions
193 and accordingly different predictive performance. For example, the study of van Wijk et al. (2008)
194 concluded that the choice of the residual function is crucial to achieve accurate model prediction
195 and parameter estimation. Shi et al. (2014) showed that the posterior parameter distributions and
196 predictive performance given by two data models (weighted least square and skew exponential
197 power distribution after removing heteroscedasticity and autocorrelation) are dramatically
198 different, and a definitive conclusion was drawn that one data model is better than the other. The
199 evaluation of predictive analysis is conducted for the following two cases: (1) the prediction
200 ensemble is generated by random samples of the soil respiration models only (i.e. credible
201 interval), and (2) the prediction ensemble is generated by random samples of not only the soil
202 respiration models but also the data models (i.e. predictive interval). The two cases lead to different
203 conclusions about the predictive performance. It is expected that the evaluation of predictive
204 performance conducted in this study can help select the most appropriate data model to achieve
205 optimal model predictions.

206 The remainder of the paper is organized as follows. Section 2 starts with a description of the
207 evolving data models and their corresponding likelihood functions used in Bayesian inference,



208 followed by a brief summary of the three soil respiration models. The results of Bayesian inference
209 are discussed in Section 3 and Section 4, addressing the data model implications on parameter
210 estimation and predictive performance, respectively. Section 5 summarizes the key findings and
211 limitations of this study, and provides recommendations for approaching data model selection.

212 **2 Methodology**

213 This section starts with a descriptions of the eight data models that account for the three pairs
214 of assumptions about residuals in a stepwise manner in Section 2.1. The data models are used to
215 build the likelihood functions used in Section 2.2 for Bayesian inference. The three soil respiration
216 models and observations of CO₂ efflux are described in Sections 2.3 and 2.4, respectively.

217 **2.1 Data models**

218 This study considers eight evolving data models starting from a data model that assumes
219 independent, homoscedastic, and Gaussian residuals to a data model that relaxes all the three
220 assumptions. The eight data models are based on the generic normalized residual,

$$221 \quad a_t = \frac{\varepsilon_t}{\sigma_t} \quad a_t \sim X, \quad (1)$$

222 where $\varepsilon_t = d_t - E_t$ is the residual (the difference between data d_t and its corresponding model
223 simulation E_t) at time or location t , σ_t is the standard deviation of the residual, and X is the
224 probability density function (PDF) of a_t . The eight data models are formulated with different forms
225 of ε_t , σ_t , and X . The standard least square (SLS) data model is

$$226 \quad a_t = \frac{\varepsilon_t}{\sigma_0} \quad a_t \sim N(0,1), \quad (2)$$

227 where $\sigma_t = \sigma_0$ is a constant for all the data (i.e., homoscedasty), and X is the standard normal
228 distribution, $N(0,1)$. The unknown parameter σ_0 is estimated jointly with unknown physical



229 model parameters. If σ_t is not a constant (i.e., heteroscedasty), SLS becomes the weighted least
230 squared (WLS) data model. While heteroscedasty can be accounted for through residuals
231 transformation (e.g. Thiemann et al., 200; Smith et al., 2010b) or other similar approaches (Gragne
232 et al., 2015) a linear heteroscedastic model $\sigma_t = \sigma_0 + \sigma_1 E_t$ is assumed following other studies
233 (Thyer et al., 2009; Schoups and Vrugt, 2010; Evin et al., 2013, 2014). With the linear model,
234 there is no need to estimate σ_t for each data. Instead, σ_t is calculated by estimating only two
235 parameters, σ_0 and σ_1 . The WSL data model is written as

$$236 \quad a_t = \frac{\varepsilon_t}{\sigma_0 + \sigma_1 E_t} \quad a_t \sim N(0,1). \quad (3)$$

237 The two unknown parameters σ_0 and σ_1 are estimated jointly with unknown physical model
238 parameters. The linear model assigns smaller weight to the data with larger simulation, E_t . If the
239 simulation is small and $\sigma_0 \gg \sigma_1 E_t$, the weight becomes constant for all data. Both SLS and WLS
240 assume that a_t is independently and identically distributed.

241 It is not uncommon that residuals are correlated in space and time, due to propagation of
242 measurement errors (Tiedeman and Green, 2013) and model structure errors (Evin et al., 2014;
243 Kavetski et al., 2013; Lu et al., 2013). The temporal correlation that occurs in the numerical
244 example of this study can be accounted for using a p -order autoregressive model. This leads to the
245 data model of standard least square with autocorrelation (SLS-AC),

$$246 \quad a_t = \frac{\varepsilon_t - \sum_{i=1}^p \phi_i \varepsilon_{t-i}}{\sigma_0} \quad a_t \sim N(0,1) \quad (4)$$



247 where p is the order of autocorrelation, and ϕ_i is an autocorrelation coefficient. The unknown ϕ_i
 248 and σ_0 are estimated together with unknown model parameters. By extending the concept of
 249 correlated residuals to WLS leads to the weight least square with autocorrelation (WLS-AC),

$$250 \quad a_t = \frac{\varepsilon_t - \sum_{i=1}^p \phi_i \varepsilon_{t-i}}{\sigma_0 + \sigma_1 E_t} \quad a_t \sim N(0,1) \quad (5)$$

251 The unknown parameters of σ_0 , σ_1 , and ϕ_i are estimated jointly with physical model
 252 parameters. Equations (2) – (5) assume that the residuals are Gaussian.

253 The next four data models are similar to the previous four models except that the standard
 254 normal distribution of a_t is replaced by the skew exponential power distribution, $SEP(0,1,\xi,\beta)$,
 255 (Schoups and Vrugt, 2010)

$$256 \quad p(a_t | \xi, \beta) = \frac{2\sigma_\xi}{\xi + \xi^{-1}} \omega_\beta \exp\left[-c_\beta |a_{\xi,t}|^{2/(1+\beta)}\right], \quad (6)$$

257 where zero is mean, one is standard deviation, ξ is skewness, β is kurtosis,

$$258 \quad a_{\xi,t} = (\mu_\xi + \sigma_\xi a_t) / \xi^{\text{sign}(\mu_\xi + \sigma_\xi a_t)}, \quad \mu_\xi = M(\xi - \xi^{-1}), \quad \omega_\beta = \frac{\Gamma^{1/2}[3(1+\beta)/2]}{(1+\beta)\Gamma^{3/2}[(1+\beta)/2]},$$

$$259 \quad \sigma_\xi = \sqrt{(1-M^2)(\xi^2 + \xi^{-2}) + 2M^2 - 1}, \quad M = \frac{\Gamma[1+\beta]}{\Gamma^{1/2}[3(1+\beta)/2]\Gamma^{1/2}[(1+\beta)/2]}, \quad \text{and}$$

$$260 \quad c_\beta = \left(\frac{\Gamma[3(1+\beta)/2]}{\Gamma[(1+\beta)/2]}\right)^{1/(1+\beta)}$$

are derived variables of β and ξ , and $\Gamma[.]$ is the gamma function. The

261 kurtosis parameter $\{\beta \in \mathbb{R} : -1 \leq \beta \leq 1\}$ determines the peakness of the pdf such that the β values
 262 of -1, 0, and 1 give uniform, Gaussian and Laplace distributions, respectively. The skewness
 263 parameter $\{\xi \in \mathbb{R} : 0.1 \leq \xi \leq 10\}$ determines the skewness of the pdf such that the ξ values of 0.1,
 264 1, and 10 give positively skewed, symmetric, and negatively skewed distributions, respectively.



265 Setting $\beta = 0$ and $\xi = 1$ leads to $\mu_\xi = 0, \sigma_\xi = 1, \omega_\beta = 1/\sqrt{2\pi}, c_\beta = 1/2$ and $a_{\xi,t} = a_t$, and the
 266 skew exponential power distribution $SEP(0,1,\xi = 1, \beta = 0)$ becomes the standard normal
 267 distribution,

$$268 \quad p(a_t | \xi = 1, \beta = 0) = \frac{1}{\sqrt{2\pi}} \exp\left[-\frac{1}{2}(a_t)^2\right]. \quad (7)$$

269 which is the data model of SLS in equation (2).

270 Replacing $a_t \sim N(0,1)$ with $a_t \sim SEP(0,1,\xi, \beta)$ in equations (2) – (5) leads to the data models
 271 SEP, WSEP, SEP-AC, and WSEP-AC as follows,

$$272 \quad a_t = \frac{\varepsilon_t}{\sigma_0} \quad a_t \sim SEP(0,1,\xi, \beta) \quad (8)$$

$$273 \quad a_t = \frac{\varepsilon_t}{\sigma_0 + \sigma_1 E_t} \quad a_t \sim SEP(0,1,\xi, \beta). \quad (9)$$

$$274 \quad a_t = \frac{\varepsilon_t - \sum_{i=1}^p \phi_i \varepsilon_{t-i}}{\sigma_0} \quad a_t \sim SEP(0,1,\xi, \beta) \quad (10)$$

$$275 \quad a_t = \frac{\varepsilon_t - \sum_{i=1}^p \phi_i \varepsilon_{t-i}}{\sigma_0 + \sigma_1 E_t} \quad a_t \sim SEP(0,1,\xi, \beta) \quad (11)$$

276 In comparison with the Gaussian data models, the SEP-based data models have two more
 277 parameters (ξ and β) to be estimated jointly with physical model parameters. WSEP-AC data
 278 model, which is known as the generalized likelihood function, is the most commonly used SEP-
 279 based data model (e.g. Vrugt and Ter Braak, 2011; Hublart et al., 2016).

280 **2.2 Bayesian inference and likelihood functions**

281 Consider a Bayesian inference problem for a nonlinear model, f , used to simulate state
 282 variables (e.g., CO₂ efflux), $\mathbf{d} = f(\boldsymbol{\theta}) + \boldsymbol{\varepsilon}$, where \mathbf{d} is a vector of data, $\boldsymbol{\theta}$ is a vector of model



283 parameters, and ε is a vector of residuals that may include errors in data, model parameters, and
 284 model structures. The goal of Bayesian inference is to estimate the posterior distributions, $p(\theta|\mathbf{d})$,
 285 of model parameters, θ , given data, \mathbf{d} , using Bayes' theorem (Box and Tiao, 1992)

$$286 \quad p(\theta|\mathbf{d}) = \frac{p(\mathbf{d}|\theta)p(\theta)}{\int p(\mathbf{d}|\theta)p(\theta)d\theta} \quad (12)$$

287 where $p(\theta)$ is the prior distribution, and $p(\mathbf{d}|\theta)$ is the likelihood function to measure goodness-of-
 288 fit between model simulations, $f(\theta)$, and data, \mathbf{d} . The prior distribution can be obtained from data
 289 of previous studies or expert judgment. When prior information is lacking, a common practice is
 290 to assume uniform distributions with relatively large parameter ranges so that the prior
 291 distributions do not affect the estimation of posterior distributions.

292 The data models above can be used to construct the likelihood functions. For the Gaussian data
 293 models given in equations (2) – (5), the corresponding Gaussian likelihood functions are
 294 straightforward, and an example is equation (7). For the SEP data models, the corresponding
 295 likelihood that is called generalized likelihood function is (Schoups and Vrugt, 2010)

$$296 \quad p(\mathbf{d}|\theta) = p(\varepsilon_t|\theta) = \prod_{t=1}^n \sigma_t^{-1} \frac{2\sigma_\xi}{\xi + \xi^{-1}} \omega_\beta \exp\left(-c_\beta |a_{\xi,t}|^{2/(1+\beta)}\right). \quad (13)$$

297 where n is the dimension of \mathbf{d} . The Gaussian likelihood functions are special case of the generalized
 298 likelihood functions. For example, by setting $\beta = 0$, $\xi = 1$, $\phi_i = 0$, $\sigma_t = \sigma_0$, $\sigma_\xi = 1$, $\mu_\xi = 0$,
 299 $\omega_\beta = 1/\sqrt{2\pi}$, $c_\beta = 1/2$, and $a_{\xi,t} = a_t$, equation (13) becomes the likelihood function corresponding
 300 to the SLS data model. Replacing $\sigma_t = \sigma_0$ by $\sigma_t = \sigma_0 + \sigma_1 E_t$, equation (13) becomes the likelihood
 301 function of the WLS data model.

302 In this study, the distributions of the data model parameters are obtained jointly with the
 303 physical model parameters using the MT-DREAM_(ZS) code (Laloy and Vrugt, 2012), which



304 implements a Markov chain Monte Carlo (MCMC) algorithm by running multiple Markov chains
305 in parallel with discrete proposal distribution, multiple-try sampling, and sampling from an
306 archive of past states. These state-of-the-art features assist in overcoming common challenges in
307 the sampling landscape such as multimodality, ill-conditioning, and high dimensionality, and thus
308 allow for accurate exploration of the targeted distributions.

309 2.3 Soil respiration models

310 Zhang et al. (2014) studied the Birch effect (the peak soil microbial respiration pulses in
311 response to episodic rainfall pulses), and developed five models, evolving from an existing four-
312 carbon pool model to models with additional carbon pools and/or explicit representations of soil
313 moisture controls on carbon degradation and microbial uptake rates. Three of the five models are
314 used in this study, and they are denoted as 4C, 5C, and 6C. Note that model 4C is model 4C_NOSM
315 of Zhang et al. (2014), not their model 4C. Figure 1 is the diagram of model 6C, the most complex
316 one among the five models. The simplest one, model 4C, has four carbon pools, i.e., soil organic
317 carbon (SOC), dissolved organic carbon (DOC), microbial biomass (MIC), and enzymes (ENZ),
318 and does not consider the soil moisture control on carbon degradation and microbial uptake rates.
319 Models 5C and 6C have an explicit representation of soil moisture controls on the rates. Based on
320 the dual Arrhenius and Michaelis–Menten kinetics model, the original SOC degradation rate,
321 V_{decom} , is (Davidson et al., 2011; Davidson and Janssens, 2006)

$$322 \quad V_{decom} = V_{max} C_{ENZ} \frac{C_{SOC}}{K_m + C_{SOC}} \quad (14)$$

323 where V_{max} [s^{-1}] is the maximum SOC degradation rate per unit enzyme when the substrate is not
324 limiting, C_{ENZ} [gCm^{-3}] is enzyme pool size, C_{SOC} [gCm^{-3}] is SOC pool size, and K_m is the half-



325 saturation for SOC. The original microbial uptake rate, V_{uptake} , is (Davidson et al., 2011; Davidson
 326 and Janssens, 2006)

$$327 \quad V_{uptake} = V_{max_up} C_{MIC} \frac{C_{DOC}}{K_{m_up} + C_{DOC}} \frac{C_{O_2}}{K_{m_upO_2} + C_{O_2}}, \quad (15)$$

328 where V_{max_up} [s^{-1}] is the maximum DOC uptake rate when the substrates is not limiting, C_{MIC}
 329 [gCm^{-3}] is the microbial biomass pool size, C_{DOC} [gCm^{-3}] is the DOC pool size, C_{O_2} [m^3m^{-3}] is
 330 the gas concentration of O_2 in the soil pore, and K_{m_up} [gCm^{-3}] and $K_{m_upO_2}$ [m^3m^{-3}] are the
 331 corresponding half-saturation constants for DOC and O_2 , respectively. With the explicit
 332 representation of soil moisture control, the two rates become (Zhang et al., 2014)

$$333 \quad V_{decom} = V_{max} C_{ENZ} \frac{C_{SOC}}{K_m + C_{SOC}} \left(\frac{\theta}{\theta_s} \right) \quad (16)$$

$$334 \quad V_{uptake} = V_{max_up} C_{MIC} \frac{C_{DOC}}{K_{m_up} + C_{DOC}} \frac{C_{O_2}}{K_{m_upO_2} + C_{O_2}} \left(\frac{\theta}{\theta_s} \right) \quad (17)$$

335 where θ [-] is the volumetric soil moisture, and θ_s [-] is the porosity.

336 In addition to using the new rate equations, models 5C and 6C have more carbon pools. In
 337 model 5C, DOC is split into two sub-pools for wet zone and dry zone of soil pores, and only the
 338 wet DOC is used by MIC, as shown in Figure 1. The moisture-controlled microbial uptake rate
 339 becomes

$$340 \quad V_{uptake} = V_{max_up} C_{MIC} \frac{C_{DOC_w}}{K_{m_up} + C_{DOC_w}} \frac{C_{O_2}}{K_{m_upO_2} + C_{O_2}} \left(\frac{\theta}{\theta_s} \right). \quad (18)$$

341 where C_{DOC_w} [gCm^{-3}] is the DOC pool size in the wet soil pores. Model 6C is more complex in
 342 that ENZ is further split into two sub-pools for wet and dry pores, and both the wet and dry ENZ



343 are subject to degradation, as shown in Figure 1. The moisture-controlled SOC degradation rate
 344 becomes

$$345 \quad V_{decom} = V_{max} C_{ENZ_W} \frac{C_{SOC}}{K_m + C_{SOC}} \left(\frac{\theta}{\theta_s} \right) \quad (19)$$

346 for the wet ENZ and

$$347 \quad V_{decom} = V_{max} C_{ENZ_D} \frac{C_{SOC}}{K_m + C_{SOC}} \left(1 - \frac{\theta}{\theta_s} \right) \varepsilon_D \quad (20)$$

348 for the dry ENZ, where C_{ENZ_W} [gCm^{-3}] is the wet soil pores enzyme pool size, C_{ENZ_D} [gCm^{-3}] is
 349 the enzyme pool size in the dry soil pores, and ε_D is the catalysis efficiency of the dry zone enzyme.

350 Due to considering the moisture control and adding more soil pools, model 5C is expected to
 351 be significantly better than model 4C for simulating the Birch effect. Since the accumulated ENZ
 352 in dry soil is secondary, model 6C is expected to be slightly better than model 5C. In terms of
 353 model structural error, model 4C has the largest model structure error, model 5C has significantly
 354 less model structure error, and model 6C has the smallest model structural error. As shown below,
 355 the degree of model structural error is reflected in the process of Bayesian inference and verified
 356 by the cross-validation.

357 **2.4 Observations and parameter estimation**

358 Figure 2 plots the time series of 17,016 observations of soil moisture and CO_2 efflux used in
 359 this study. The observations were obtained during the entire year of 2007, covering a long period
 360 of dry season prior to monsoon and episodic rainfall events during monsoon. The first two third of
 361 this dataset is used for the Bayesian inference, and the last one third is used for cross-validation.
 362 The inference and cross-validation periods have both dry and wet periods, as shown in Figure 2.
 363 The observation site is located within the Santa Rita Experimental Range (SRER, 31.8214°N ,



364 110.8661°W, elevation 1,116 m) outside of Tucson, Arizona (Barron-Gafford et al., 2011; Scott
365 et al., 2009). This savanna site was covered by 22% of perennial grass, forbs and subshrubs and
366 35% of mesquite. The soils are uniformly Comoro loamy sand (77.6% sand, 11.0% clay, and
367 11.4% silt). The half-hourly atmospheric forcing data were collected from measurements through
368 an eddy covariance tower (Scott et al., 2009). This includes downward shortwave, longwave,
369 precipitation, wind, air temperature, humidity, and pressure. Volumetric CO₂ concentration was
370 measured at half-hourly interval through compact probes. The CO₂ efflux was estimated from the
371 gradient of CO₂ concentration measured at two depths of 2 cm and 10 cm through Fick's first law
372 of diffusion, and the estimates were validated against measurements from a portable CO₂ gas
373 analyzer.

374 The parameters estimated in this study include the parameters of the soil respiration models
375 (4C – 6C) and the parameters of the data models described in Section 2.1. The estimated
376 parameters of models 4C and 5C include the microbial carbon use efficiency (CUE) [g/g], enzyme
377 production rate, k_e [g/m³s], microbial turnover rate, τ_m [1/s], and enzyme turnover rate τ_e [1/s].
378 Uniform distributions are used as the prior in the Bayesian inference, and the ranges of the four
379 parameters are 0.2 – 1.00, 1×10^{-12} – 1×10^{-7} , 1×10^{-12} – 1×10^{-5} and 1×10^{-11} – 1×10^{-6} , respectively.
380 The values of other parameters are fixed at the values used in Allison et al. (2010). Model 6C has
381 two more parameters, and they are the catalysis efficiency ε_D [-] and the turnover rate of the dry-
382 zone enzymes τ_{en} [1/s]. The prior of the two parameters are uniform distributions with the ranges
383 of 0.2 – 0.8 and 1×10^{-12} – 1×10^{-8} , respectively.

384 The DREAM-based MCMC simulation is conducted for a total of 24 cases, the combinations
385 of eight data models and three physical models. For each case, the parameter distributions are
386 obtained after drawing a total of 5×10^5 samples using five Markov chains. The Gelman and Rubin



387 (1992) R-statistic is used for convergence diagnostic, and it approaches one in less than 4×10^4
388 samples. The initial 50% of the samples are discarded during the burn-in period.

389 **3 Results of Bayesian Inverse Modeling**

390 This section analyzes the residuals of the best realization (with the highest likelihood value) of
391 the MCMC simulation to understand whether the assumptions of the eight data models hold. The
392 impacts of the data models on the posterior parameter distributions are also analyzed.

393 **3.1 Residual characterization**

394 Figure 3 shows residual plots for model 6C based on data models SLS and WSEP-AC. SLS is
395 the simplest one with the assumptions of homoscedastic, independent, and Gaussian residuals, and
396 the WSEP-AC is the most complex one without the assumptions. Model 6C is the most complex
397 model and also the best one as ranked by Zhang et al. (2014) using Bayesian model selection. The
398 variable a_t plotted in Figures 3a-3c and Figures 3d-3f is defined in equations (2) and (11),
399 respectively. Figures 3a – 3c show that the three residual assumptions are violated when SLS is
400 used because (i) the residual variance is not constant, but increases as a function of the simulated
401 CO₂ efflux (Figure 3a); (ii) the autocorrelation function at most lags is beyond the 95% confidence
402 interval (Figure 3b); (iii) and the standard normal density function cannot adequately characterize
403 the residuals (Figure 3c). Figures 3d-f show that, after relaxing the three assumptions, the
404 processed residuals, a_t , can be well characterized by WSEP-AC. Figure 3d shows that, after
405 normalizing ε_t with the linear variance ($\sigma_t = 0.034 + 0.099 E_t$), the variation of the variance of
406 a_t becomes significantly smaller, although the variance is still not a constant. Figure 3e shows that,
407 after removing a first-order autoregressive model from ε_t , a_t becomes less correlated, although the
408 correlation is not fully removed. The two coefficients of the autoregressive model are $\phi_1 = 0.989$
409 and $\phi_2 = 4.5 \times 10^{-6}$; the small value of ϕ_2 indicates that there is no need to attempt an autoregressive



410 model of higher order. Figure 3f shows that a_t follows the SEP distribution with the estimated
411 skewness coefficient of $\xi = 0.933$ and kurtosis coefficient of $\beta = 0.998$. As a summary, Figure
412 3 shows that it is important to examine the residuals and to determine whether a data model is
413 adequate for charactering the residuals. Although WSEP-AC still cannot perfectly characterize ε_t ,
414 it is significantly better than SLS.

415 Although the Gaussian assumption used in SLS is violated for model 4C (Figure 3c), this is
416 not generally the case for other data models and physical models. This is shown in Figure 4, which
417 presents the quantile-quantile (Q-Q) plot for the eight data models and the three soil respiration
418 models. For SLS, WLS, SLS-AC, and WLS-AC, the theoretical quantiles are based on the standard
419 normal distribution, $N(0,1)$; for SEP, WSEP, SEP-AC, and WSEP-AC, the theoretical quantiles
420 are based on the standard skew exponential power distribution, $SEP(0,1,1,0)$. If the residuals
421 follow the assumed standard distributions, the Q-Q plots fall on the 1:1 line, which is marked as
422 the theoretical lines in Figure 4. If the residuals are Gaussian or SEP but not standard, the Q-Q
423 plots fall on a straight line but not the 1:1 line. Figures 4a and 4e show that, for all the soil
424 respiration models, the Q-Q plots of SLS and SEP deviate significantly from the theoretical lines
425 and exhibit fat-tail behaviors, which is an indication of outliers (Thyer et al., 2009). The deviation
426 is reduced after accounting for autocorrelation in SLS-AC and SEP-AC, as shown in Figures 4c
427 and 4g (it is interesting to observe from the two figures that the Q-Q plots of the three models are
428 almost visually identical). The deviation is almost fully removed after accounting for
429 heteroscedasticity in WLS and WSEP in that their corresponding Q-Q plots fall on the 1:1 lines,
430 especially for models 5C and 6C, as shown in Figures 4b and 4f. However, the Q-Q plots start
431 deviating from the 1:1 lines as shown in Figures 4d and 4h, after accounting for both
432 heteroscedasticity and autocorrelation in WLS-AC and WSEP-AC. As a summary, Figure 4 shows



433 that, for the numerical example of this study, either the Gaussian or the SEP distribution is valid if
434 heteroscedasticity is accounted for in the data models. However, accounting for autocorrelation in
435 the data models does not help improve the characterization of the residual distribution.

436 **3.2 Posterior parameter distributions**

437 While Figures 3 and 4 help understand validity of the three assumptions used in the data
438 models, the impacts of the data models on estimating model parameter distributions must be
439 evaluated separately. This section discusses the impact of the data model selection on parameter
440 estimation with the objective of understanding if incorrect specification of the data model, will
441 necessarily lead to biased parameter estimates. Such assessment is not a trivial task for three main
442 reasons. First, microbial soil respiration models aggregate complex natural processes and spatial
443 details into simpler conceptual representations. As a results several model parameters are effective
444 values of several complex natural processes that cannot be actually measured in the field as
445 discussed by Vrugt et al. (2013). Second, even for model parameter that can be measured in the
446 field, since the model structure is imperfect, it can be the case that parameter values can be
447 accepted beyond their physically reasonable range as discussed by Pappengerger and Beven
448 (2006). This is often undesirable, if we seek to make the models more mechanistically descriptive.

449 We focus our discussion on carbon use efficiency (CUE) for microbial growth since CUE is a
450 fundamental parameter in microbial soil respiration models, and a reasonable physical range for
451 CUE can estimated. The concept of microbial CUE(Allison et al., 2010; Bradford et al., 2008;
452 Manzoni et al., 2012; Wieder et al., 2013) has been used to present fundamental microbial
453 processes recent microbial enzyme models(Allison et al., 2010; German et al., 2011; Schimel and
454 Weintraub, 2003; Wang et al., 2013). The microbial CUE, which is marked between MIC and CO₂
455 in Figure 1, controls microbial growth, enzyme production and microbial respiration. A reasonable



456 range of CUE can be estimated from the physical viewpoint(Tang and Riley, 2014). Sinsabaugh
457 et al. (2013) study shows that the thermodynamic calculations support a maximum CUE of 0.60
458 and that methods used to estimate CUE in terrestrial systems report a mean value of 0.55.
459 Theoretically, there no lower limit for CUE as it can approach zero, and $CUE < 0.1$ are reported
460 for terrestrial ecosystems (e.g. Fernández-Martínez et al., 2014) and used in modeling studies (Li
461 et al., 2014).

462 Figure 5 plots the CUE posterior marginal density of the three soil respiration models obtained
463 using the eight data models. The physical range between zero and 0.6 is marked in yellow. Figure
464 5 shows that the CUE posterior parameter distribution for Model 6C for all likelihood functions
465 that does not account for autocorrelation are within a reasonable physical range. For models 4C
466 and 5C, the posterior parameter samples are outside the physical range for six data models. For
467 model 4C, the posterior parameters are within the physical range only for data models SEP and
468 WSEP; for model 5C, the two data models are WLS and WSEP. It is not surprising to find the
469 posterior parameter distribution of models 4C and 5C, which have a certain degree of model
470 structure error, to be out of the plausible physical range. This can be attributed to two reasons.
471 First, the model solution can be biased toward the missing processes in the model structure such
472 as the additional carbon pool in both 4C and 5C or the explicit accounting for soil moisture in 4C.
473 Second, biased parameter estimation can compensate for model structure inadequacy and other
474 sources of discrepancy in both the physical model and the statistical model.

475 In addition, it is important to understand how accounting for autocorrelation, heteroscedasty
476 and non-Gaussian residuals can affect the parameter estimation. First, it is not unexpected to get
477 biased parameter estimates that can be out the reasonable physical range when autocorrelation is
478 explicitly accounted for as shown in Figure 5e-h. This may suggest again that accounting for



479 heteroscedasticity is desirable but accounting for autocorrelation is not. A possible reason is that
480 filtering autocorrelation may reduce the residual space such that the transformed residual space
481 cannot correspond to the parameter space of the models. In other words, parameter information
482 may be lost due to filtering out autocorrelation. However, it is not fully understood why this does
483 not occur for the model 6C under data model SLS-AC, and more research is warranted. Second,
484 unlike accounting for auto-correlation, accounting only for heteroscedasty (i.e. WLS and WSEP)
485 since this will only amplify or reduce the variance without affecting the structure of the residual
486 space. Figure 5c-d shows that account for heteroscedasty (i.e. WLS and WSEP) tends to improve
487 the parameter estimation in comparison with homoscedastic data models (i.e. SLS and SEP) shown
488 in Figure 5a-b. Finally, with respect to non-Gaussian residuals, Schoups and Vrugt (2010)
489 proposes that the peaked pdf of the SEP with heavier tails compared to Gaussian pdf is useful for
490 making parameter inference robust against outliers. To a certain degree, this can be substantiated
491 by the results in Figure 5a-d, such that SEP and WSEP provide more favorable parameter estimates
492 than SLS and WLS.

493 Finally, from Figure 5 we can also notice that the posterior parameter distribution of SLS
494 (Figure 5a) is very narrow. This narrow posterior parameter distribution of SLS compared to other
495 likelihood functions can be attributed to several reasons. Since SEP can have heavier tails than
496 Gaussian distribution, this can further increase the samples acceptance ratio from tails resulting in
497 wider distribution (Figure 5b). In addition, accounting for heteroscedasticity will wider the
498 posterior parameter distribution (Figure 5c) due to accepting higher variances at peak effluxes.
499 Moreover, filtering correlation (Figure 5e-h) increases the entropy.



500 4. Results of Predictive Performance

501 Based on the last one third of the CO₂ efflux observations, a cross-validation test was conducted
502 for all the 24 models, the combinations of three soil respiration models and eight data models.
503 Given the cross-validation data, the predictive performance is examined using the four statistical
504 metrics defined in Section 4.1. The metrics are also calculated for the calibration data. This is not
505 to perform Bayesian model selection given the calibration data, but to better understand the impact
506 of data models. For each calibration and each cross-validation data, a prediction ensemble is
507 generated from the two perspectives of parametric uncertainty only and total uncertainty, as
508 presented in Section 4.2 and 4.3, respectively.

509 4.1 Metrics for evaluating predictive performance

510 Three criteria are used to evaluate the predictive performance of the soil respiration models
511 and data models, and they are central mean tendency, dispersion, and reliability. Each criteria is
512 measured by a single metric. In addition, a newly defined metric is also used for simultaneously
513 measuring the three criteria. The central mean tendency is measured in this study using the Nash-
514 Sutcliffe model efficiency (NSME) coefficient (Nash and Sutcliffe, 1970),

$$515 \quad NSME = 1 - \frac{\sum_{i=1}^n (d_i - \overline{X_i})^2}{\sum_{i=1}^n (d_i - \overline{\mathbf{d}})^2}, \quad (21)$$

516 where n is the number of cross-validation data, d_i is the i -th data, $\overline{\mathbf{d}}$ is the mean of the data, and
517 $\overline{X_i}$ is the mean of the prediction ensemble, X_i , for d_i . NSME ranges from $-\infty$ to 1, with $NSME = 1$
518 corresponding to a perfect match between data and mean prediction, i.e., the ensemble is centered
519 on the data. $NSME = 0$ indicates that the model predictions are as only accurate as the mean of the
520 data, while an efficiency $NSME < 1$ indicates that the mean of data is a better prediction than the
521 mean prediction.



522 In addition to the central mean tendency, it is also desirable that the ensemble is precise with
 523 small dispersion and reliable to cover all the data. This study uses a nonparametric metric for
 524 dispersion, and it is the sharpness of a prediction interval (e.g. Smith et al., 2010a)

$$525 \quad \textit{Sharpness} = 1/n \sum_{i=1}^n [\textit{Max}(X_i) - \textit{Min}(X_i)] \quad (22)$$

526 where X_i is the prediction ensemble within the 95% prediction interval (the Bayesian credible
 527 interval, not the confidence interval used in nonlinear regression (Lu et al., 2013). Smaller values
 528 of sharpness indicate better prediction precision. Reliability is measured using predictive coverage.
 529 (e.g. Hoeting et al., 1999), which is the percentages of data contained in the prediction interval.
 530 Larger predictive coverage values are preferred.

531 To account for the trade-off between the three metrics,(Elshall et al., 2018) defined relative
 532 model score (RMS) that simultaneously measure all the three criteria. Scoring rules are commonly
 533 used in hydrology to assess predictive performance (e.g. Weijs et al., 2010; Westerberg et al.,
 534 2011). RMS is used in this study to measure the relative predictive performance of the
 535 combinations of soil respiration models and data models. For combination M_j , RMS is defined as

$$536 \quad \textit{RMS}(M_j) = \frac{\sum_{i=1}^n p(d_i | X_{ij}, M_j)}{\sum_{j=1}^m p(d_i | X_{ij}, M_j)} \times 100 \quad (23)$$

537 where $m = 24$ is the number of combinations, and X_{ij} is similar to X_i above and specific to the j -th
 538 combination. The density function, $p(d_i|X_{ij})$, can be evaluated by first obtaining the density function
 539 $p(X_{ij})$ of the ensemble prediction X_{ij} (e.g., by using the kernel density function) and then evaluating
 540 $p(d_i|X_{ij})$ using interpolation methods based on the intersection of X_{ij} and d_i . This evaluation is based
 541 purely on the model predictions, and does not involve any assumptions on the models, their
 542 parameters, and likelihood functions. Larger RMS values indicate better overall predictive
 543 performance.



544 4.2 Predictive performance with parametric uncertainty of soil respiration models

545 In this section the ensemble is generated by running the soil respiration models with the
546 posterior samples (obtained from the Bayesian inference) of the physical model parameters. In
547 other words, the ensemble addresses parametric uncertainty of the soil respiration models only.
548 Considering the relative contribution of parametric uncertainty only will provide insights for
549 modeling approaches that attempt to segregate various sources of uncertainty (e.g. Thyer et al.,
550 2009; Elshall and Tsai, 2014).

551 The four statistics above (i.e. NSME, sharpness, coverage, and RMS) are calculated for the
552 three soil respiration models and the eight data models. Taking data models SLS and WSEP-AC
553 as an example, Figure 6 plots the data (for the calibration and cross-validation periods separately)
554 along with the mean and 95% credible intervals of the prediction ensemble for the three models.

555 Figure 6 shows that the data models affect model simulations for all the models. The statistics,
556 especially RMS, indicate that WSEP-AC has better predictive performance than SLS. This is most
557 visually obvious for model 6C during the cross-validation period after 330 days, as the prediction
558 ensemble of SLS (Figure 6k) cannot cover the observations unlike the prediction ensemble of
559 WSEP-AC can (Figure 6l). This conclusion that WSEP-AC outperforms SLS agrees with that
560 drawn from Figures 3 and 4.

561 Figure 7 plots the four statistics for all the soil respiration models and data models. Figures 7a
562 and 7b show the predictive performance with respect to the central mean tendency using NSME
563 for both the calibration and cross-validation periods respectively. The results indicates that the
564 low fidelity model 4C under all data models will over-fit the data resulting in biased predictions
565 such that the NSME values become significantly worse (from 0.6 to -0.6) from the calibration to
566 the cross-validation period. This is confirmed by the visual inspection of Figures 6a, 6b, 6g, and



567 6h for data models SLS and WSEP-AC. For models 5C and 6C, their NSME values vary with the
568 data models with the central mean accuracy being the worst for SLS-AC which considers only
569 autocorrelation.

570 With respect to parametric uncertainty estimation, Figures 7c and 7d show sharpness generally
571 increases when the three assumptions in the data models are gradually relaxed from SLS to WSEP-
572 AC. This is even more obvious during the validation period. Given that the prediction ensemble
573 does not center on the data, the increasing sharpness is desirable as it improves reliability. This is
574 confirmed by the reliability plots in Figures 7e and 7f. The exceptions are again SLS-AC and SEP-
575 AC that generally have the lowest coverage.

576 With respect to the overall predictive performance, the same variation pattern and exception
577 are also observed in the RMS plots in Figures 7g and 7h. This is not surprising because RMS is
578 the metric that can be used to measure all the three criteria (central mean tendency, sharpness, and
579 reliability). Since the prediction ensemble is not centered on the data, the sharpness and reliability
580 are the decisive factors for evaluating the predictive performance.

581 As a summary, while it is necessary to account for heteroscedasticity in a data model, caution
582 is needed when accounting for autocorrelation in the manner described in Section 2.1. In addition,
583 after comparing the RMS values of the residuals using the Gaussian and SEP distributions. The
584 conclusion is that the SEP distribution outperforms the Gaussian distribution with respect to
585 predictive performance. Finally, uncertainty underestimation as evident by the very small
586 predictive coverage. The underestimation of uncertainty for all the physical models with all
587 likelihood function make sense because only parametric uncertainty is considered. Considering
588 the overall predictive uncertainty is the subject of the next section.



589 **4.3 Predictive performance with parametric uncertainty of soil respiration models and**
590 **data models**

591 The simulated output $\mathbf{Y}(\theta_p)$ will generally not be equally to the observed output \mathbf{D} and we
592 have a residue error term \mathbf{e} due to measurement, input and model structure errors such that
593 $\mathbf{D} = \mathbf{Y}(\theta_p) + \mathbf{e}$. Accounting for error term \mathbf{e} can be through separating various error terms. For
594 example, in section 4.2 we obtained uncertainty due to the physical model parameters. Accounting
595 for other sources of uncertainty can be done using a single model approach (e.g. Thyer et al., 2009)
596 or a multimodel approach (e.g. Tsai and Elshall, 2013). Alternatively, we can quantify the
597 uncertainty based on total residuals, which include measurement, model input, model structure and
598 parameter estimation errors (e.g. Thyer et al., 2009; Schoups and Vrugt, 2010). This lumped
599 approach is based on sampling the residual error model $\mathbf{e}(\theta_e)$ with parameters θ_e . SLS has one
600 fixed parameter that is the constant variance and other data models have two to six parameters.
601 Thus in Section 4.3, the prediction ensemble addresses parametric uncertainty of not only the soil
602 respiration models but also the data models. When generating the prediction ensemble in the
603 procedure described by Schoups and Vrugt (2010), an ensemble of residuals is first generated by
604 running the data models with posterior samples of the data model parameters for the positive
605 carbon efflux domain; the residual ensemble is then added to the prediction ensemble generated in
606 Section 4.2.

607 We start by the visual assessment of the predictive performance. Figure 8 is similar to Figure
608 6 with the exception that Figure 8 considers the overall all predictive uncertainty (i.e. parametric
609 and output uncertainty), while Figure 6 considers the parametric uncertainty only. Figure 8 reveals
610 a practical observation about accounting for the overall uncertainty through the lumped approach
611 of sampling the residual errors model. Figure 8b shows that despite the wide prediction interval



612 of model 4C, which has significant model structure error, it could not capture the birch pulse
613 around day 180. This clearly indicates that proper modeling of the residual error will not make-up
614 for of significant model structure error.

615 Figure 9 plots the four statistics (NSME, sharpness, predictive coverage, and RMS) of the three
616 models under the eight data models to assess the predictive performance. First with respect to
617 central mean tendency, The NSME values in Figures 9a-9b are visually the same as those in
618 Figures 7a-7b, indicating that the central mean accuracy under parametric uncertainty is the same
619 as that under predictive uncertainty.

620 With respect to uncertainty, the values of sharpness and predictive coverage increase
621 substantially (Figures 9c – 9f). In particular, Figures 9e and 9f show that, except for SLS and SEP,
622 the predictive coverage of the rest six data models are close to 100% for all the three models,
623 indicating that the prediction intervals cover almost all the data. This is demonstrated in Figures 6
624 for WSEP-AC. Similar to Figures 7c and 7d, Figures 9c and 9d also show a general pattern that
625 the sharpness increases when the three assumptions in the data models are gradually relaxed from
626 SLS to WSEP-AC. The data models that account for autocorrelation are still the exceptions.

627 With respect to the overall predictive performance, the RMS values are largely determined by
628 mean accuracy and sharpness as the predictive coverage is similar for different data models.
629 Figures 9g and 9h of RMS show that the predictive performance of the four data models that
630 account for autocorrelation is worse than that of the other four data models. This suggests again
631 that one needs to be cautious when building autocorrelation into a data model. This is consistent
632 with the finding of Evin et al. (2013, 2014) that accounting for autocorrelation before accounting
633 for heteroscedasticity or jointly accounting for autocorrelation and heteroscedasticity can result in
634 poor predictive performance. In summary, Figures 9g and 9h show for both the calibration and



635 prediction periods that accounting for heteroscedasticity (i.e. WLS and WSEP) will give the best
636 overall predictive skill, and accounting for autocorrelation without heteroscedasticity (i.e. SLS-
637 AC and SEP-AC) will give the worst overall predictive skill. Finally, for the three soil respiration
638 models, RMS shows that model 4C has the worst predictive performance for both the calibration
639 and cross-validation data. Generally speaking, the high fidelity model 6C outperforms model 5C
640 for both the calibration and cross-validation data, which justifies the complexity of model 6C.

641 To demonstrate the impacts of the data models on predictive performance of the soil respiration
642 models, Figure 10 plots the model simulations and predictions given by model 6C during the
643 calibration and cross-validation periods using all the eight data models.

644 In Figure 10 we try to understand the predictive performance characteristics of the different
645 data models by looking at the predictive performance of model 6C. Specific predictive
646 performance patterns can be identified. Figures 10-a-d show that SLS and SEP have similar
647 predictive performance with SEP generally having better predictive skill especially during the
648 validation period. Accounting for heteroscedasticity using WLS as shown in Figures 10e and 10h
649 will make the predictions more sensitive to peak carbon effluxes and will generally improve the
650 predictive coverage on the expense of sharpness and the central mean tendency. WLS and WSEP
651 have similar predictive performance. However, WSEP maintains slightly better central mean
652 tendency and overall predictive performance than WLS. Accounting for autocorrelation using
653 SLS-AC and SEP-AC as shown in Figures 10i and 10l reduces the information content of the
654 residuals thus resulting in wider uncertainty bands and insensitivity to peak carbon effluxes as
655 compared to SLS and SEP (Figures 10a-d). This resulted in deteriorating the sharpness, the central
656 mean tendency and the capturing of peak carbon fluxes, especially during the validation period.
657 Accounting for both heteroscedasticity and autocorrelation using WLS-AC and WSEP-AC will



658 make the inference robust against peck carbon effluxes, yet due to the loss of information content
659 uncertainty bands are still wider and uncertainty becomes overestimated especially during
660 validation period as compared to WLS and WSEP. The results of Models 4C and 5C, which are
661 not shown here, also show the same prediction patterns with respect to non-Gaussian residuals,
662 heteroscedasticity and autocorrelation.

663 From figure 10 we also notice that data models that have good overall predictive performance
664 as measured by RMS during the calibration period will maintain this good predictive performance
665 during the validation period. For model 6C, RMS values for the calibration and validation periods
666 are very well correlated with a correlation coefficient of 0.92. However, we note that for models
667 4C and 5C the overall predictive performance during the calibration and validation periods are not
668 that well correlated as 6C, with correlation coefficients of 0.52 for model 4C and 0.61 for model
669 5C. This suggests that model 6C is more robust than 4C and 5C for forecasting and hindcasting.

670 **5. Conclusions**

671 In parameter estimation and prediction of soil carbon fluxes to the atmosphere we often
672 assume that residuals, which include observation, model input, model structure and parameter
673 estimation errors, are normally distributed, homoscedastic and uncorrelated. We studied these
674 assumptions by calibrating three microbial enzyme models, which have varying degrees of model
675 structure errors. We tested eight data modeling starting with the standard least squares (SLS) and
676 skew exponential power (SEP) data models that assume homoscedastic and non-correlated
677 residuals. Given these two distributions, we evaluated six other data models that account for
678 heteroscedasticity (WLS and WSEP), autocorrelation (SLS-AC and SEP-AC) and joint inversion of
679 heteroscedasticity and autocorrelation (WLS-AC and WSEP-AC). To our knowledge this is the first
680 study that provide such detailed analysis soil respiration inverse modeling. We also used three solid



681 respiration models with different degrees of model realism and model complexity (i.e. number of
682 model parameters), to understand the impact of model discrepancy on the calibration results under
683 different data models. We analyzed the calibration results with respect to (i) residual
684 characterization, (ii) parameter estimation, (iii) predictive performance and (iv) impact of model
685 discrepancy. The main findings of this study can be summarized as follows:

686 (i) With respect to residual characterization, residual analysis results suggest that the common
687 assumption of not accounting for heteroscedasticity and autocorrelation of residuals (i.e. SLS and
688 SEP) results in poor characterization of residuals. Explicit accounting for heteroscedasticity (i.e.
689 WLS and WSEP) can result in good characterization of the residuals, and is followed by joint the
690 inversion of heteroscedasticity and autocorrelation (i.e. WSL-AC and WSEP-AC). Accounting for
691 autocorrelation only (i.e. SLS-AC and SEP-AC) may not improve much the characterization of the
692 residuals.

693 (ii) With respect to parameter estimation, we focused on carbon use efficiency (CUE), which
694 is a central parameter in soil respiration modeling. We found the SLS with relatively reasonable
695 posterior parameter distribution for CUE, yet very narrow posterior. Data models consider
696 autocorrelation (i.e. SLS-AC, SEP-AC, WLS-AC and WSEP-AC) tend to generally yield CUE
697 estimates that are physically non-reasonable. We speculate that filtering correlation can affect the
698 mapping of the model physics (as implicitly included in the residuals) into the likelihood space,
699 which might result in biased parameter estimates that are physically unreasonable.

700 (iii) With respect to predictive performance, we assessed the central mean tendency,
701 uncertainty bands and the overall predictive performance for both the calibration and the cross-
702 validation periods. Results show that accounting for autocorrelation (i.e. SLS-AC, SEP-AC, WLS-
703 AC, and WSEP-AC) deteriorate the predicative performance, such that the predictive performance



704 is inferior to SLS in terms of the central mean tendency and overall predictive skill, especially
705 during the cross-validation period. Results also indicates that using a SEP distribution can
706 potentially improve the predictive performance. The same is true for accounting for
707 heteroscedasticity. Using SEP distribution and accounting for heteroscedasticity (i.e. WSEP) can
708 potentially improve the predictive performance.

709 (iv) With respect to the impact of model discrepancy, the high fidelity complex model (6C)
710 gives the best results with respect to parameter estimation and predictive performance. Model 6C
711 generally maintained its superior performance under different data models. This justifies the
712 complexity of model 6C relative to model 5C that has one less carbon pool. Model 4C that has a
713 low fidelity model with only four carbon pools and lacks the explicit representation of soil moisture
714 control, maintains its poor performance for different data models.

715 From the empirical findings of this research we conclude the following: (i) Not accounting for
716 heteroscedasticity and autocorrelation using a Gaussian or non-Gaussian data model might not
717 necessarily result in biased parameter estimates or biased predictions with respect to central mean
718 tendency, but will definitely underestimate uncertainty resulting in lower overall predictive
719 performance. (ii) Using a non-Gaussian residual error model can improve the parameter estimates,
720 and the predictive performance with respect to central mean tendency and uncertainty estimation.
721 (iii) Accounting for heteroscedasticity will definitely improve the uncertainty estimation with
722 respect to reliability at the cost of having a wider predictive interval. (iv) This study confirms the
723 empirical findings and theoretical analysis of Evin et al. (2013; 2014) that separate accounting for
724 autocorrelation or joint inversion of correlation and heteroscedasticity can be problematic.
725 Relatively poor performance with respect to autocorrelation can be due to our implementation
726 scheme, which can be improved by using the post-processing inference approach for



727 autocorrelation (Evin et al., 2013; 2014) or similar strategies (Li et al., 2015, 2016). Further
728 investigation of this point is warranted in a future study.

729 The conclusions above are subject to several limitations. First, the conclusions are specific to
730 the soil respiration models developed and validated for semi-arid savannah. Performance
731 variations across different soil respiration models with different levels of complexities is possible.
732 Second, the conclusions are conditioned on the data that were obtained at the half-hour interval
733 over a one-year period. Different conclusions are possible if the data are thinned to daily or weekly
734 scales or data of longer observation periods are used. Third, the study investigates effects of the
735 residual assumptions of formal likelihood functions through direct conditioning of the error model
736 parameters, yet this can also be done through other approaches such as residuals transformation
737 (Thiemann et al., 2001), autoregressive bias model (Del Giudice et al., 2013), approximate Bayesian
738 computation (Sadegh and Vrugt, 2013), data assimilation (Spaaks and Bouten, 2013). Comparing
739 different methods for accounting the residual assumptions are beyond the scope of this work.
740 Fourth, this study focuses on formal Bayesian computation using formal likelihood functions, and
741 comparison with other inference functions such as informal likelihood functions or approximate
742 Bayesian computation is warranted in a future study.

743 Based on the aforesaid conclusions and limitations, we recommend to start calibrating soil
744 respiration models with simple SLS or SEP likelihood function. If the residuals characterization is
745 adequate (e.g. Scharnagl et al., 2011), then the underlying assumptions are met. Otherwise,
746 increase complexity of the data model until satisfactory results are obtained in terms of residuals
747 characterization, posterior parameter estimation and predictive performance. Although the
748 empirical findings of this study provide general guidelines for data model selection of microbial



749 soil respiration models, more comparative studies are needed to validate and refute the findings of
750 this study.

751 **Code and data availability**

752 The data and codes and models used to produce this paper are available on contact of the
753 corresponding author at mye@fsu.edu. We cannot publicly share the workflow because MT-
754 DREAM_(ZS) code (Laloy and Vrugt, 2012), which is a main component in the workflow, is in the
755 process of becoming a commercial code.

756 **Author contributions**

757 ASE developed and implemented the code for the eight data models for soil respiration modeling,
758 and prepared the manuscript with contribution of all co-authors. MY developed the research idea
759 and outline, and supervised the research implementation. GN developed the soil respiration
760 models. GAB collected and processed the eddy-covariance data used for model calibration.

761 **Competing interests**

762 The authors declare that they have no conflict of interest.

763 **Acknowledgement**

764 This work was supported by the Department of Energy Early Career Award, DE-SC0008272 and
765 U.S. National Science Foundation Award# OIA-1557349.

766 **References**

767 Ahrens, B., Reichstein, M., Borken, W., Muhr, J., Trumbore, S. E. and Wutzler, T.: Bayesian
768 calibration of a soil organic carbon model using ΔC measurements of soil organic carbon
769 and heterotrophic respiration as joint constraints, *Biogeosciences*, 11(8), 2147–2168,
770 doi:10.5194/bg-11-2147-2014, 2014.

771 Allison, S. D., Wallenstein, M. D. and Bradford, M. A.: Soil-carbon response to warming



- 772 dependent on microbial physiology, *Nat. Geosci.*, 3, 336 [online] Available from:
773 <http://dx.doi.org/10.1038/ngeo846>, 2010.
- 774 Barr, J. G., Engel, V., Fuentes, J. D., Fuller, D. O. and Kwon, H.: Modeling light use efficiency in
775 a subtropical mangrove forest equipped with CO₂ eddy covariance, *Biogeosciences*, 10(3),
776 2145–2158, doi:10.5194/bg-10-2145-2013, 2013.
- 777 Barron-Gafford, G. A., Scott, R. L., Jenerette, G. D. and Huxman, T. E.: The relative controls of
778 temperature, soil moisture, and plant functional group on soil CO₂ efflux at diel,
779 seasonal, and annual scales, *J. Geophys. Res. Biogeosciences*, 116(1), 1–16,
780 doi:10.1029/2010JG001442, 2011.
- 781 Bradford, M. A., Davies, C. A., Frey, S. D., Maddox, T. R., Melillo, J. M., Mohan, J. E., Reynolds,
782 J. F., Treseder, K. K. and Wallenstein, M. D.: Thermal adaptation of soil microbial
783 respiration to elevated temperature, *Ecol. Lett.*, 11(12), 1316–1327, doi:10.1111/j.1461-
784 0248.2008.01251.x, 2008.
- 785 Chevallier, F. and O'Dell, C. W.: Error statistics of Bayesian CO₂ flux inversion schemes as seen
786 from GOSAT, *Geophys. Res. Lett.*, 40(6), 1252–1256, doi:10.1002/grl.50228, 2013.
- 787 Davidson, E. A. and Janssens, I. A.: Temperature sensitivity of soil carbon decomposition and
788 feedbacks to climate change, *Nature*, 440, 165 [online] Available from:
789 <http://dx.doi.org/10.1038/nature04514>, 2006.
- 790 Davidson, E. A., Samanta, S., Caramori, S. S. and Savage, K.: The Dual Arrhenius and Michaelis–
791 Menten kinetics model for decomposition of soil organic matter at hourly to seasonal time
792 scales, *Glob. Chang. Biol.*, 18(1), 371–384, doi:10.1111/j.1365-2486.2011.02546.x, 2011.
- 793 Elshall, A. S. and Tsai, F. T.-C.: Constructive epistemic modeling of groundwater flow with
794 geological structure and boundary condition uncertainty under the Bayesian paradigm, *J.*



- 795 Hydrol., 517, doi:10.1016/j.jhydrol.2014.05.027, 2014.
- 796 Elshall, A. S., Ye, M., Pei, Y., Zhang, F., Niu, G.-Y. and Barron-Gafford, G. A.: Relative model
797 score: a scoring rule for evaluating ensemble simulations with application to microbial soil
798 respiration modeling, *Stoch. Environ. Res. Risk Assess.*, 32(10), 2809–2819,
799 doi:10.1007/s00477-018-1592-3, 2018.
- 800 Evin, G., Kavetski, D., Thyer, M. and Kuczera, G.: Pitfalls and improvements in the joint inference
801 of heteroscedasticity and autocorrelation in hydrological model calibration, *Water Resour.*
802 *Res.*, 49(7), 4518–4524, doi:10.1002/wrcr.20284, 2013.
- 803 Evin, G., Thyer, M., Kavetski, D., McInerney, D. and Kuczera, G.: Comparison of joint versus
804 postprocessor approaches for hydrological uncertainty estimation accounting for error
805 autocorrelation and heteroscedasticity, *Water Resour. Res.*, 50(3), 2350–2375,
806 doi:10.1002/2013WR014185, 2014.
- 807 Fernández-Martínez, M., Vicca, S., Janssens, I. A., Sardans, J., Luysaert, S., Campioli, M.,
808 Chapin III, F. S., Ciais, P., Malhi, Y., Obersteiner, M., Papale, D., Piao, S. L., Reichstein,
809 M., Rodà, F. and Peñuelas, J.: Nutrient availability as the key regulator of global forest
810 carbon balance, *Nat. Clim. Chang.*, 4, 471 [online] Available from:
811 <http://dx.doi.org/10.1038/nclimate2177>, 2014.
- 812 Gelman, A. and Rubin, D. B.: Inference from Iterative Simulation Using Multiple Sequences, *Stat.*
813 *Sci.*, 7(4), 457–472, doi:10.1214/ss/1177011136, 1992.
- 814 German, D. P., Marcelo, K. R. B., Stone, M. M. and Allison, S. D.: The Michaelis–Menten kinetics
815 of soil extracellular enzymes in response to temperature: a cross-latitude study, *Glob.*
816 *Chang. Biol.*, 18(4), 1468–1479, doi:10.1111/j.1365-2486.2011.02615.x, 2011.
- 817 Del Giudice, D., Honti, M., Scheidegger, A., Albert, C., Reichert, P. and Rieckermann, J.:



- 818 Improving uncertainty estimation in urban hydrological modeling by statistically describing
819 bias, *Hydrol. Earth Syst. Sci.*, 17(10), 4209–4225, doi:10.5194/hess-17-4209-2013, 2013.
- 820 Gragne, A. S., Sharma, A., Mehrotra, R. and Alfredsen, K.: Improving real-time inflow forecasting
821 into hydropower reservoirs through a complementary modelling framework, *Hydrol. Earth*
822 *Syst. Sci.*, 19(8), 3695–3714, doi:10.5194/hess-19-3695-2015, 2015.
- 823 Hararuk, O., Xia, J. and Luo, Y.: Evaluation and improvement of a global land model against soil
824 carbon data using a Bayesian Markov chain Monte Carlo method, *J. Geophys. Res.*
825 *Biogeosciences*, 119(3), 403–417, doi:10.1002/2013JG002535, 2014.
- 826 Hashimoto, S., Morishita, T., Sakata, T., Ishizuka, S., Kaneko, S. and Takahashi, M.: Simple
827 models for soil CO₂, CH₄, and N₂O fluxes calibrated using a Bayesian approach and multi-
828 site data, *Ecol. Modell.*, 222(7), 1283–1292, doi:10.1016/j.ecolmodel.2011.01.013, 2011.
- 829 Hilton, T. W., Davis, K. J. and Keller, K.: Evaluating terrestrial CO₂ flux diagnoses and
830 uncertainties from a simple land surface model and its residuals, *Biogeosciences*, 11(2), 217–
831 235, doi:10.5194/bg-11-217-2014, 2014.
- 832 Hoeting, J. A., Madigan, D., Raftery, A. E. and Volinsky, C. T.: Bayesian model averaging: a
833 tutorial (with comments by M. Clyde, David Draper and E. I. George, and a rejoinder by the
834 authors, *Stat. Sci.*, 14(4), 382–417, doi:10.1214/ss/1009212519, 1999.
- 835 Högberg, P. and Read, D. J.: Towards a more plant physiological perspective on soil ecology,
836 *Trends Ecol. Evol.*, 21(10), 548–554, doi:10.1016/j.tree.2006.06.004, 2006.
- 837 Hublart, P., Ruelland, D., De Cortázar-Atauri, I. G., Gascoin, S., Lhermitte, S. and Ibacache, A.:
838 Reliability of lumped hydrological modeling in a semi-arid mountainous catchment facing
839 water-use changes, *Hydrol. Earth Syst. Sci.*, 20(9), 3691–3717, doi:10.5194/hess-20-3691-
840 2016, 2016.



- 841 Janssens, I. A., Freibauer, A., Ciais, P., Smith, P., Nabuurs, G.-J., Folberth, G., Schlamadinger, B.,
842 Hutjes, R. W. A., Ceulemans, R., Schulze, E.-D., Valentini, R. and Dolman, A. J.: Europe's
843 terrestrial biosphere absorbs 7 to 12% of European anthropogenic CO₂ emissions., *Science*,
844 300(5625), 1538–42, doi:10.1126/science.1083592, 2003.
- 845 Katz, R. W., Craigmile, P. F., Guttorp, P., Haran, M., Sansó, B. and Stein, M. L.: Uncertainty
846 analysis in climate change assessments, *Nat. Clim. Chang.*, 3, 769 [online] Available from:
847 <http://dx.doi.org/10.1038/nclimate1980>, 2013.
- 848 Kavetski, D., Franks, S. W. and Kuczera, G.: Confronting Input Uncertainty in Environmental
849 Modelling, *Calibration Watershed Model.*, doi:doi:10.1029/WS006p0049, 2013.
- 850 Keenan, T. F., Davidson, E., Moffat, A. M., Munger, W. and Richardson, A. D.: Using model-data
851 fusion to interpret past trends, and quantify uncertainties in future projections, of terrestrial
852 ecosystem carbon cycling, *Glob. Chang. Biol.*, 18(8), 2555–2569, doi:10.1111/j.1365-
853 2486.2012.02684.x, 2012.
- 854 Klemedtsson, L., Jansson, P. E., Gustafsson, D., Karlberg, L., Weslien, P., Von Arnold, K.,
855 Ernfors, M., Langvall, O. and Lindroth, A.: Bayesian calibration method used to elucidate
856 carbon turnover in forest on drained organic soil, *Biogeochemistry*, 89(1), 61–79,
857 doi:10.1007/s10533-007-9169-0, 2008.
- 858 Laloy, E. and Vrugt, J. A.: High-dimensional posterior exploration of hydrologic models using
859 multiple-try DREAM(ZS) and high-performance computing, *Water Resour. Res.*, 48(1),
860 doi:10.1029/2011WR010608, 2012.
- 861 Li, J., Wang, G., Allison, S. D., Mayes, M. A. and Luo, Y.: Soil carbon sensitivity to temperature
862 and carbon use efficiency compared across microbial-ecosystem models of varying
863 complexity, *Biogeochemistry*, 119, 67–84 [online] Available from:



- 864 <http://www.jstor.org/stable/24716883>, 2014.
- 865 Li, M., Wang, Q. J., Bennett, J. C. and Robertson, D. E.: A strategy to overcome adverse effects
866 of autoregressive updating of streamflow forecasts, *Hydrol. Earth Syst. Sci.*, 19(1), 1–15,
867 doi:10.5194/hess-19-1-2015, 2015.
- 868 Li, M., Wang, Q. J., Bennett, J. C. and Robertson, D. E.: Error reduction and representation in
869 stages (ERRIS) in hydrological modelling for ensemble streamflow forecasting, *Hydrol.*
870 *Earth Syst. Sci.*, 20(9), 3561–3579, doi:10.5194/hess-20-3561-2016, 2016.
- 871 Lu, D., Ye, M., Meyer, P. D., Curtis, G. P., Shi, X., Niu, X.-F. and Yabusaki, S. B.: Effects of error
872 covariance structure on estimation of model averaging weights and predictive performance,
873 *Water Resour. Res.*, 49(9), 6029–6047, doi:10.1002/wrcr.20441, 2013.
- 874 Luo, Y., Ogle, K., Tucker, C., Fei, S., Gao, C., LaDeau, S., Clark, J. S. and Schimel, D. S.:
875 Ecological forecasting and data assimilation in a data-rich era, *Ecol. Appl.*, 21(5), 1429–
876 1442, doi:10.1890/09-1275.1, 2011.
- 877 Luo, Y., Keenan, T. F. and Smith, M.: Predictability of the terrestrial carbon cycle, *Glob. Chang.*
878 *Biol.*, 21(5), 1737–1751, doi:10.1111/gcb.12766, 2014.
- 879 Manzoni, S., Taylor, P., Richter, A., Porporato, A. and Ågren, G. I.: Environmental and
880 stoichiometric controls on microbial carbon-use efficiency in soils, *New Phytol.*, 196(1), 79–
881 91, doi:10.1111/j.1469-8137.2012.04225.x, 2012.
- 882 Nash, J. E. and Sutcliffe, J. V: River flow forecasting through conceptual models part I — A
883 discussion of principles, *J. Hydrol.*, 10(3), 282–290, doi:[https://doi.org/10.1016/0022-](https://doi.org/10.1016/0022-1694(70)90255-6)
884 [1694\(70\)90255-6](https://doi.org/10.1016/0022-1694(70)90255-6), 1970.
- 885 Pappenberger, F. and Beven, K. J.: Ignorance is bliss: Or seven reasons not to use uncertainty
886 analysis, *Water Resour. Res.*, 42(5), doi:10.1029/2005WR004820, 2006.



- 887 Peters, W., Jacobson, A. R., Sweeney, C., Andrews, A. E., Conway, T. J., Masarie, K., Miller, J.
888 B., Bruhwiler, L. M. P., Pétron, G., Hirsch, A. I., Worthy, D. E. J., van der Werf, G. R.,
889 Randerson, J. T., Wennberg, P. O., Krol, M. C. and Tans, P. P.: An atmospheric perspective
890 on North American carbon dioxide exchange: CarbonTracker., Proc. Natl. Acad. Sci. U. S.
891 A., 104(48), 18925–30, doi:10.1073/pnas.0708986104, 2007.
- 892 Le Quéré, C., Peters, G. P., Andres, R. J., Andrew, R. M., Boden, T. A., Ciais, P., Friedlingstein,
893 P., Houghton, R. A., Marland, G., Moriarty, R., Sitch, S., Tans, P., Arneeth, A., Arvanitis, A.,
894 Bakker, D. C. E., Bopp, L., Canadell, J. G., Chini, L. P., Doney, S. C., Harper, A., Harris, I.,
895 House, J. I., Jain, A. K., Jones, S. D., Kato, E., Keeling, R. F., Klein Goldewijk, K.,
896 Körtzinger, A., Koven, C., Lefèvre, N., Maignan, F., Omar, A., Ono, T., Park, G.-H., Pfeil,
897 B., Poulter, B., Raupach, M. R., Regnier, P., Rödenbeck, C., Saito, S., Schwinger, J.,
898 Segschneider, J., Stocker, B. D., Takahashi, T., Tilbrook, B., van Heuven, S., Viovy, N.,
899 Wanninkhof, R., Wiltshire, A. and Zaehle, S.: Global carbon budget 2013, Earth Syst. Sci.
900 Data, 6(1), 235–263, doi:10.5194/essd-6-235-2014, 2014.
- 901 Raich, J. W. J. J. W., Potter, C. S. C. and Bhagawati, D.: Interannual variability in global soil
902 respiration, 1980-94, Glob. Chang. Biol., 8, 800–812, doi:10.1046/j.1365-
903 2486.2002.00511.x, 2002.
- 904 Ren, X., He, H., Moore, D. J. P., Zhang, L., Liu, M., Li, F., Yu, G. and Wang, H.: Uncertainty
905 analysis of modeled carbon and water fluxes in a subtropical coniferous plantation, J.
906 Geophys. Res. Biogeosciences, 118(4), 1674–1688, doi:10.1002/2013JG002402, 2013.
- 907 Ricciuto, D. M., King, A. W., Dragoni, D. and Post, W. M.: Parameter and prediction uncertainty
908 in an optimized terrestrial carbon cycle model: Effects of constraining variables and data
909 record length, J. Geophys. Res. Biogeosciences, 116(1), 1–17, doi:10.1029/2010JG001400,



- 910 2011.
- 911 Richardson, A. D. and Hollinger, D. Y.: Statistical modeling of ecosystem respiration using eddy
912 covariance data: Maximum likelihood parameter estimation, and Monte Carlo simulation of
913 model and parameter uncertainty, applied to three simple models, *Agric. For. Meteorol.*,
914 131(3–4), 191–208, doi:10.1016/j.agrformet.2005.05.008, 2005.
- 915 Sadegh, M. and Vrugt, J. A.: Bridging the gap between GLUE and formal statistical approaches:
916 Approximate Bayesian computation, *Hydrol. Earth Syst. Sci.*, 17(12), 4831–4850,
917 doi:10.5194/hess-17-4831-2013, 2013.
- 918 Scharnagl, B., Vrugt, J. A., Vereecken, H. and Herbst, M.: Inverse modelling of in situ soil water
919 dynamics: Investigating the effect of different prior distributions of the soil hydraulic
920 parameters, *Hydrol. Earth Syst. Sci.*, 15(10), 3043–3059, doi:10.5194/hess-15-3043-2011,
921 2011.
- 922 Schimel, J. P. and Weintraub, M. N.: The implications of exoenzyme activity on microbial carbon
923 and nitrogen limitation in soil: a theoretical model, *Soil Biol. Biochem.*, 35(4), 549–563,
924 doi:10.1016/S0038-0717(03)00015-4, 2003.
- 925 Schmidt, M. W. I., Torn, M. S., Abiven, S., Dittmar, T., Guggenberger, G., Janssens, I. A., Kleber,
926 M., Kögel-Knabner, I., Lehmann, J., Manning, D. A. C., Nannipieri, P., Rasse, D. P., Weiner,
927 S. and Trumbore, S. E.: Persistence of soil organic matter as an ecosystem property, *Nature*,
928 478(7367), 49–56, doi:10.1038/nature10386, 2011.
- 929 Schoups, G. and Vrugt, J. A.: A formal likelihood function for parameter and predictive inference
930 of hydrologic models with correlated, heteroscedastic, and non-Gaussian errors, *Water*
931 *Resour. Res.*, 46(10), 1–17, doi:10.1029/2009WR008933, 2010.
- 932 Scott, R. L., Jenerette, G. D., Potts, D. L. and Huxman, T. E.: Effects of seasonal drought on net



- 933 carbon dioxide exchange from a woody-plant-encroached semiarid grassland, *J. Geophys.*
934 *Res. Biogeosciences*, 114(4), doi:10.1029/2008JG000900, 2009.
- 935 Shi, X., Ye, M., Curtis, G. P., Miller, G. L., Meyer, P. D., Kohler, M., Yabusaki, S. and Wu, J.:
936 Assessment of parametric uncertainty for groundwater reactive transport modeling, *Water*
937 *Resour. Res.*, 50(5), 4416–4439, doi:10.1002/2013WR013755, 2014.
- 938 Sinsabaugh, R. L., Manzoni, S., Moorhead, D. L. and Richter, A.: Carbon use efficiency of
939 microbial communities: stoichiometry, methodology and modelling, *Ecol. Lett.*, 16(7), 930–
940 939, doi:10.1111/ele.12113, 2013.
- 941 Smith, M. W., Bracken, L. J. and Cox, N. J.: Toward a dynamic representation of hydrological
942 connectivity at the hillslope scale in semiarid areas, *Water Resour. Res.*, 46(12),
943 doi:10.1029/2009WR008496, 2010a.
- 944 Smith, T., Sharma, A., Marshall, L., Mehrotra, R. and Sisson, S.: Development of a formal
945 likelihood function for improved Bayesian inference of ephemeral catchments, *Water*
946 *Resour. Res.*, 46(12), 1–11, doi:10.1029/2010WR009514, 2010b.
- 947 Smith, T., Marshall, L. and Sharma, A.: Modeling residual hydrologic errors with Bayesian
948 inference, *J. Hydrol.*, 528, 29–37, doi:10.1016/j.jhydrol.2015.05.051, 2015.
- 949 Spaaks, J. H. and Bouten, W.: Resolving structural errors in a spatially distributed hydrologic
950 model using ensemble Kalman filter state updates, *Hydrol. Earth Syst. Sci.*, 17(9), 3455–
951 3472, doi:10.5194/hess-17-3455-2013, 2013.
- 952 Steinacher, M. and Joos, F.: Transient Earth system responses to cumulative carbon dioxide
953 emissions: Linearities, uncertainties, and probabilities in an observation-constrained model
954 ensemble, *Biogeosciences*, 13(4), 1071–1103, doi:10.5194/bg-13-1071-2016, 2016.
- 955 Tang, J. and Riley, W. J.: Weaker soil carbon–climate feedbacks resulting from microbial and



- 956 abiotic interactions, *Nat. Clim. Chang.*, 5, 56 [online] Available from:
957 <http://dx.doi.org/10.1038/nclimate2438>, 2014.
- 958 Tang, J. and Zhuang, Q.: A global sensitivity analysis and Bayesian inference framework for
959 improving the parameter estimation and prediction of a process-based Terrestrial Ecosystem
960 Model, *J. Geophys. Res. Atmos.*, 114(D15), doi:10.1029/2009JD011724, 2009.
- 961 Thiemann, M., Trosset, M., Gupta, H. and Sorooshian, S.: Bayesian recursive parameter estimation
962 for hydrologic models, *Water Resour. Res.*, 37(10), 2521–2535,
963 doi:10.1029/2000WR900405, 2001.
- 964 Thyer, M., Renard, B., Kavetski, D., Kuczera, G., Franks, S. W. and Srikanthan, S.: Critical
965 evaluation of parameter consistency and predictive uncertainty in hydrological modeling: A
966 case study using Bayesian total error analysis, *Water Resour. Res.*, 45(12), 1–22,
967 doi:10.1029/2008WR006825, 2009.
- 968 Tiedeman, C. R. and Green, C. T.: Effect of correlated observation error on parameters,
969 predictions, and uncertainty, *Water Resour. Res.*, 49(10), 6339–6355,
970 doi:10.1002/wrcr.20499, 2013.
- 971 Tsai, F. T.-C. and Elshall, A. S.: Hierarchical Bayesian model averaging for hydrostratigraphic
972 modeling: Uncertainty segregation and comparative evaluation, *Water Resour. Res.*, 49(9),
973 doi:10.1002/wrcr.20428, 2013.
- 974 Tucker, C. L., Young, J. M., Williams, D. G. and Ogle, K.: Process-based isotope partitioning of
975 winter soil respiration in a subalpine ecosystem reveals importance of rhizospheric
976 respiration, *Biogeochemistry*, 121, 389–408 [online] Available from:
977 <http://www.jstor.org/stable/24717586>, 2014.
- 978 Tuomi, M., Vanhala, P., Karhu, K., Fritze, H. and Liski, J.: Heterotrophic soil respiration-



- 979 Comparison of different models describing its temperature dependence, *Ecol. Modell.*,
980 211(1–2), 182–190, doi:10.1016/j.ecolmodel.2007.09.003, 2008.
- 981 Vargas, R., Carbone, M. S., Reichstein, M. and Baldocchi, D. D.: Frontiers and challenges in soil
982 respiration research: from measurements to model-data integration, *Biogeochemistry*,
983 102(1), 1–13, doi:10.1007/s10533-010-9462-1, 2011.
- 984 Vrugt, J. A. and Ter Braak, C. J. F.: DREAM(D): An adaptive Markov Chain Monte Carlo
985 simulation algorithm to solve discrete, noncontinuous, and combinatorial posterior parameter
986 estimation problems, *Hydrol. Earth Syst. Sci.*, 15(12), 3701–3713, doi:10.5194/hess-15-
987 3701-2011, 2011.
- 988 Vrugt, J. A., ter Braak, C. J. F., Diks, C. G. H. and Schoups, G.: Hydrologic data assimilation using
989 particle Markov chain Monte Carlo simulation: Theory, concepts and applications, *Adv.*
990 *Water Resour.*, 51, 457–478, doi:10.1016/j.advwatres.2012.04.002, 2013.
- 991 Wang, G., Post, W. M. and Mayes, M. A.: Development of microbial-enzyme-mediated
992 decomposition model parameters through steady-state and dynamic analyses, *Ecol. Appl.*,
993 23(1), 255–272, doi:10.1890/12-0681.1, 2013.
- 994 Weijs, S. V., Schoups, G. and Van De Giesen, N.: Why hydrological predictions should be
995 evaluated using information theory, *Hydrol. Earth Syst. Sci.*, 14(12), 2545–2558,
996 doi:10.5194/hess-14-2545-2010, 2010.
- 997 Westerberg, I. K., Guerrero, J. L., Younger, P. M., Beven, K. J., Seibert, J., Halldin, S., Freer, J.
998 E. and Xu, C. Y.: Calibration of hydrological models using flow-duration curves, *Hydrol.*
999 *Earth Syst. Sci.*, 15(7), 2205–2227, doi:10.5194/hess-15-2205-2011, 2011.
- 1000 Wieder, W. R., Bonan, G. B. and Allison, S. D.: Global soil carbon projections are improved by
1001 modelling microbial processes, *Nat. Clim. Chang.*, 3, 909 [online] Available from:



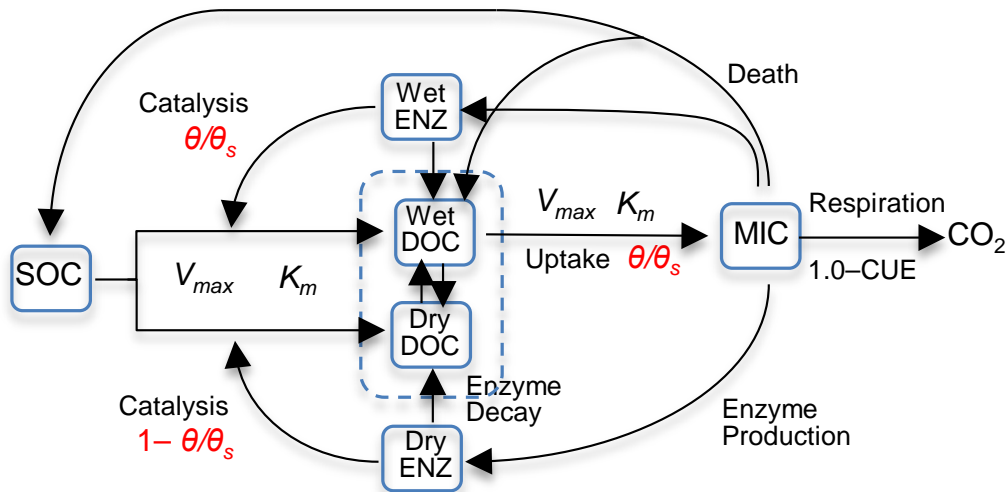
- 1002 <http://dx.doi.org/10.1038/nclimate1951>, 2013.
- 1003 Wieder, W. R., Allison, S. D., Davidson, E. A., Georgiou, K., Hararuk, O., He, Y., Hopkins, F.,
1004 Luo, Y., Smith, M. J., Sulman, B., Todd-Brown, K., Wang, Y.-P., Xia, J. and Xu, X.:
1005 Explicitly representing soil microbial processes in Earth system models, *Global*
1006 *Biogeochem. Cycles*, 29(10), 1782–1800, doi:10.1002/2015GB005188, 2015.
- 1007 Van Wijk, M. T., Van Putten, B., Hollinger, D. Y. and Richardson, A. D.: Comparison of different
1008 objective functions for parameterization of simple respiration models, *J. Geophys. Res.*
1009 *Biogeosciences*, 113(3), 1–11, doi:10.1029/2007JG000643, 2008.
- 1010 Xu, T., White, L., Hui, D. and Luo, Y.: Probabilistic inversion of a terrestrial ecosystem model:
1011 Analysis of uncertainty in parameter estimation and model prediction, *Global Biogeochem.*
1012 *Cycles*, 20(2), 1–15, doi:10.1029/2005GB002468, 2006.
- 1013 Xu, X., Schimel, J. P., Thornton, P. E., Song, X., Yuan, F. and Goswami, S.: Substrate and
1014 environmental controls on microbial assimilation of soil organic carbon: a framework for
1015 Earth system models, *Ecol. Lett.*, 17(5), 547–555, doi:10.1111/ele.12254, 2014.
- 1016 Yeluripati, J. B., van Oijen, M., Wattenbach, M., Neftel, A., Ammann, A., Parton, W. J. and Smith,
1017 P.: Bayesian calibration as a tool for initialising the carbon pools of dynamic soil models,
1018 *Soil Biol. Biochem.*, 41(12), 2579–2583, doi:10.1016/j.soilbio.2009.08.021, 2009.
- 1019 Zhang, X., Niu, G.-Y., Elshall, A. S., Ye, M., Barron-Gafford, G. A. and Pavao-Zuckerman, M.:
1020 Assessing five evolving microbial enzyme models against field measurements from a
1021 semiarid savannah - What are the mechanisms of soil respiration pulses?, *Geophys. Res.*
1022 *Lett.*, 41(18), doi:10.1002/2014GL061399, 2014.
- 1023 Zhou, X., Luo, Y., Gao, C., Verburg, P. S. J., Arnone, J. A., Darrouzet-Nardi, A. and Schimel, D.
1024 S.: Concurrent and lagged impacts of an anomalously warm year on autotrophic and



1025 heterotrophic components of soil respiration: A deconvolution analysis, *New Phytol.*, 187(1),
1026 184–198, doi:10.1111/j.1469-8137.2010.03256.x, 2010.
1027



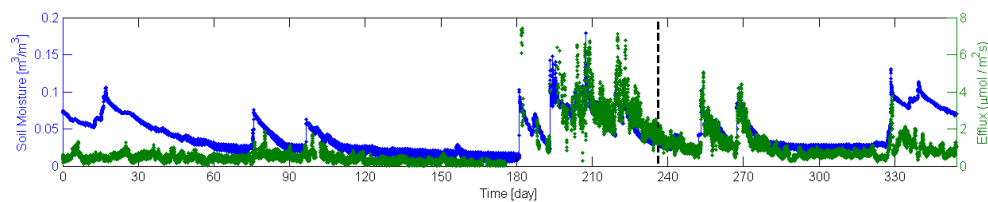
1028 Figure 1. Diagram of model 6C representing the processes of (1) degradation of soil organic carbon
 1029 (SOC) to dissolved organic carbon (DOC) through catalysis of enzymes (ENZ) produced by
 1030 microbes (MIC), (2) MIC uptake of DOC, and (3) microbial (MIC) respiration to produce CO₂
 1031 (CUE is the carbon use efficiency). SOC degradation and microbial uptake rates are controlled by
 1032 water saturation (θ / θ_s). The DOC and ENZ pools are split into two subpools, one for the wet zone
 1033 and the other for the dry zone of the soil pore space. Microbial uptake of DOC occurs only in the
 1034 wet zone, and the uptake rate is linearly related to θ / θ_s . Catalysis through ENZ in the wet zone is
 1035 proportional to θ / θ_s , while that in the dry zone is proportional to $1 - \theta / \theta_s$. V_{max} (s⁻¹) is the maximum
 1036 rate, and K_m is the half-saturation concentration.
 1037



1038
 1039



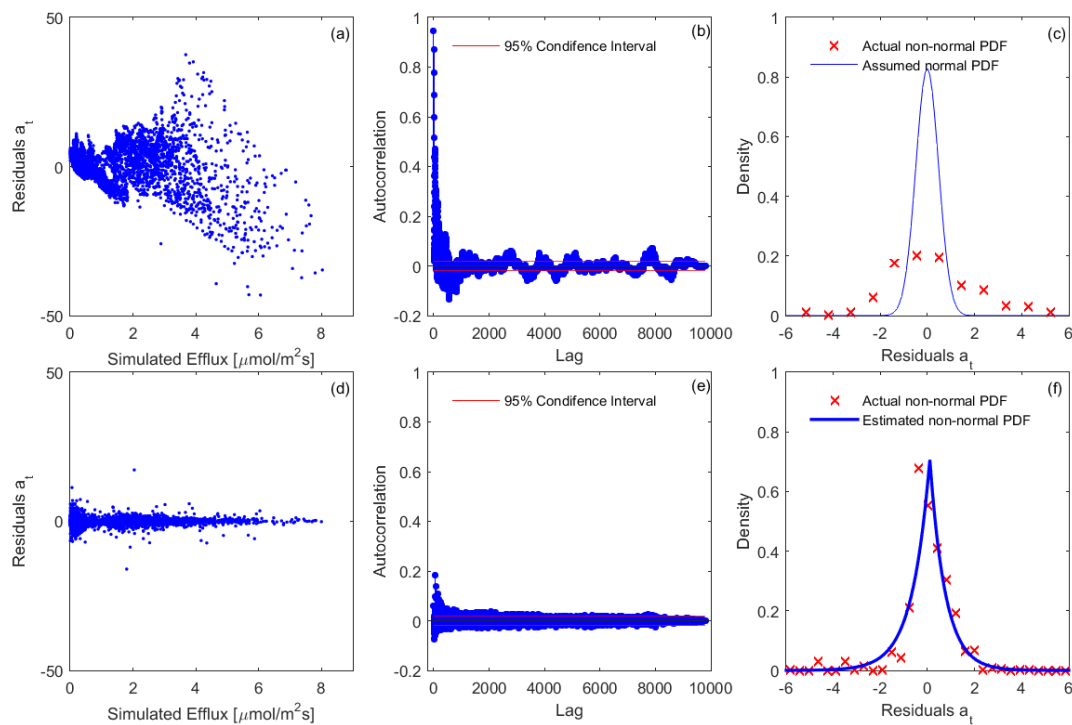
1040 Figure 2. Time series of soil moisture and efflux observations. The dashed line marks the divide
1041 of the dataset into calibration and validation periods.
1042



1043



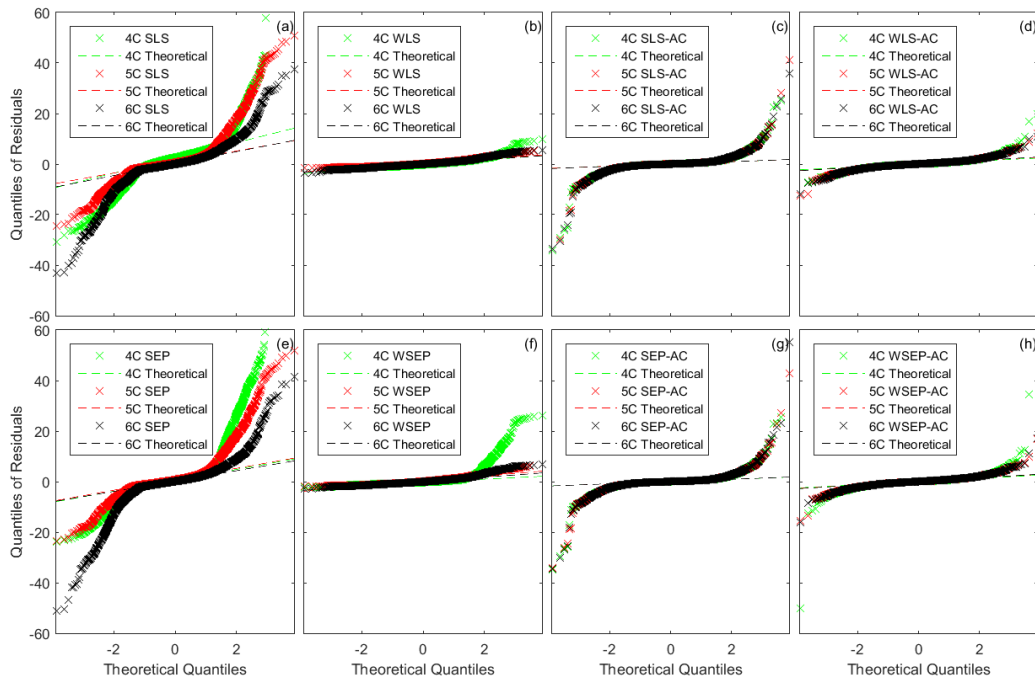
1044 Figure 3. Residual analysis of the best realization (among multiple MCMC realizations) for model
1045 6C using data models (a-c) SLS and (d-f) WSEP-AC.
1046



1047



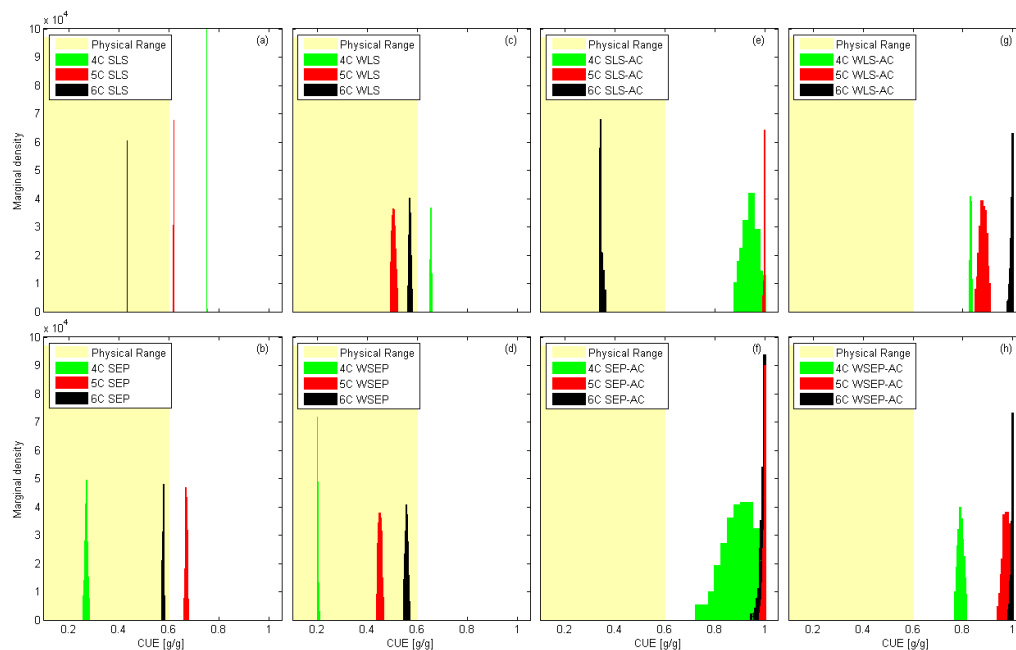
1048 Figure 4. Residual quantile-quantile (Q-Q) plots of the best realization (among multiple MCMC
1049 realizations) for the three soil respiration models and eight data models.
1050



1051



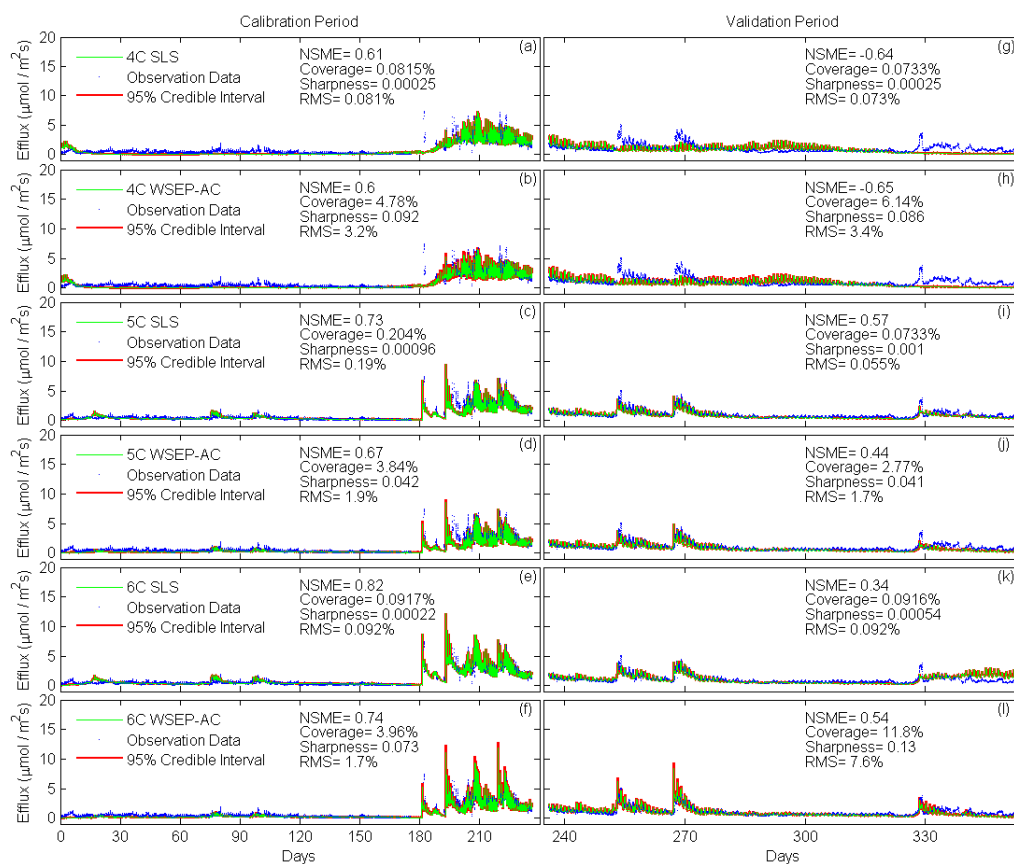
1052 Figure 5. Marginal posterior parameter density of carbon use efficiency (CUE) for the three soil
1053 respiration models and eight data models.
1054



1055



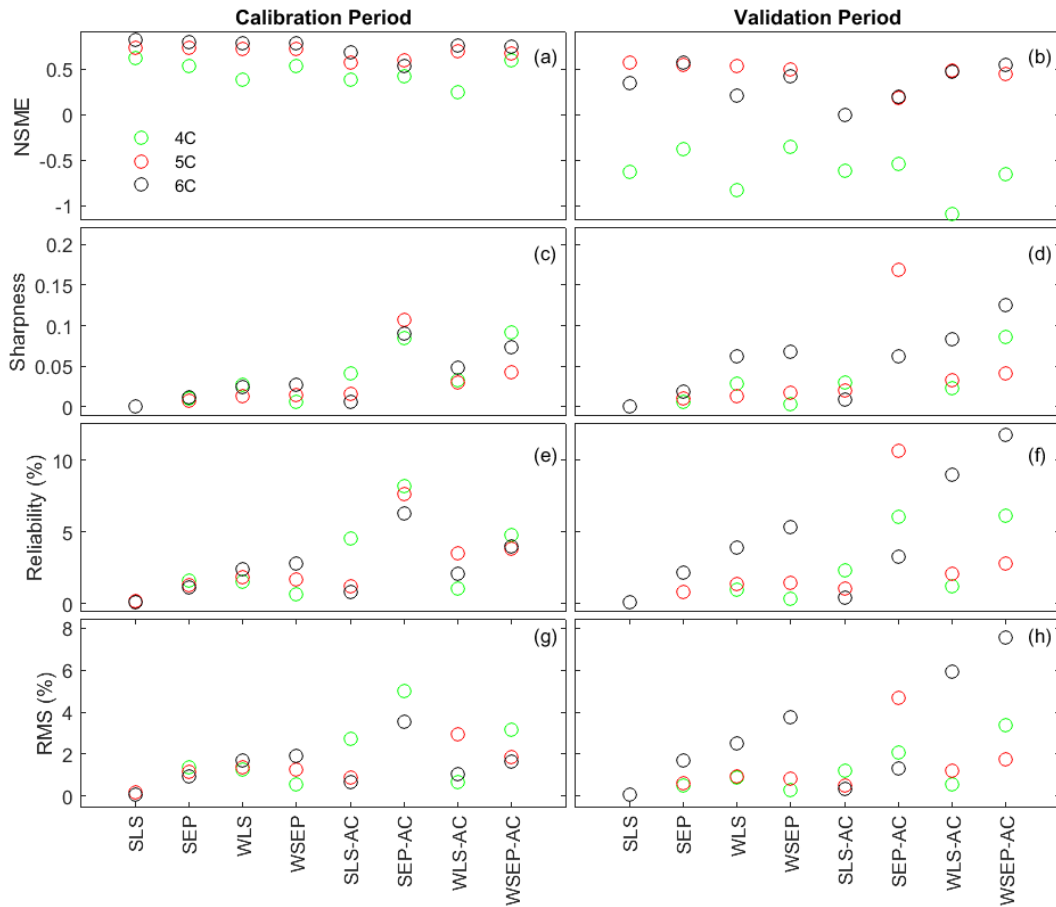
1056 Figure 6. Observation data (blue dots) and mean prediction (green line) and 95% credible intervals
 1057 (red line) of prediction ensembles for (a)-(f) the calibration period and (g)-(l) the validation period.
 1058 The plots are for the three soil respiration models using data models SLS and WSEP-AC. *The prediction ensembles are generated to consider parametric uncertainty of the soil respiration*
 1059 *models only.*
 1060
 1061



1062



1063 Figure 7. (a-b) Nash-Sutcliffe model efficiency (NSME), (c)-(d) sharpness, (e)-(f) predictive
 1064 coverage, and (g)-(h) relative model score for measuring predictive performance of the three soil
 1065 respiration models and the eight data models during the calibration and cross-validation periods.
 1066 *The statistics are evaluated from the prediction ensembles generated to consider parametric*
 1067 *uncertainty of the soil respiration models only.*
 1068

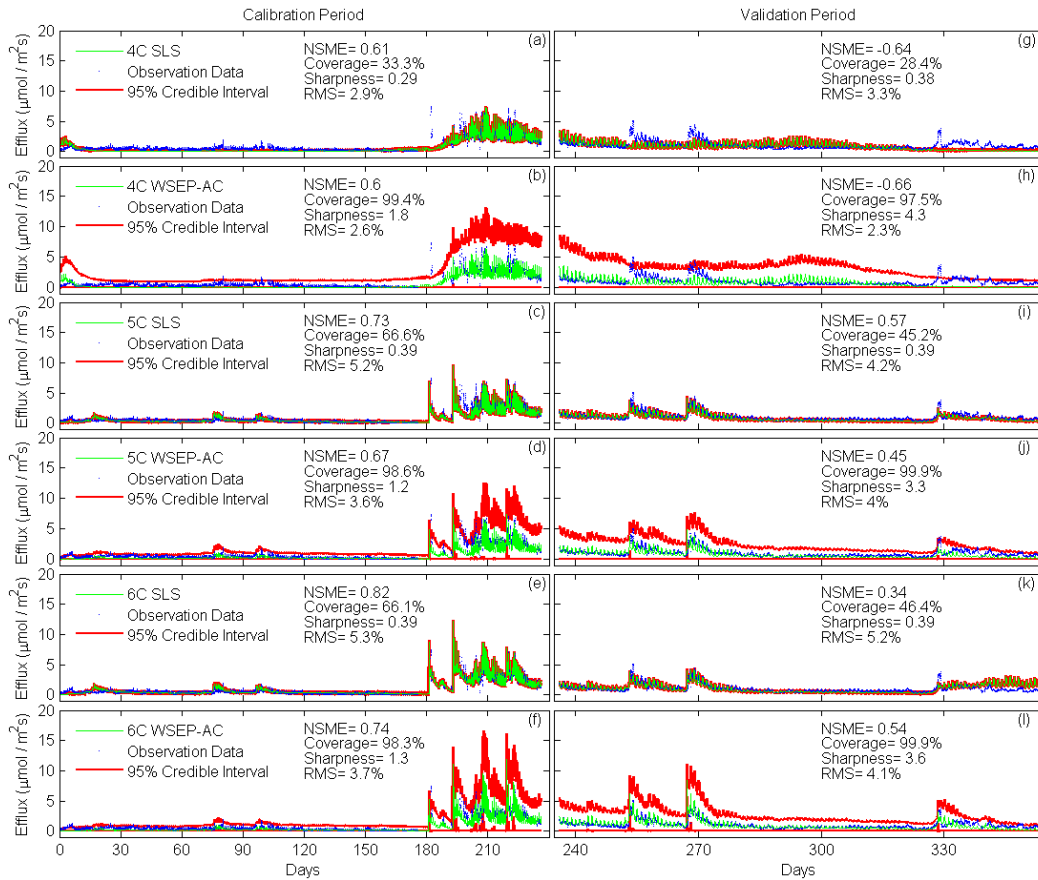


1069

1070



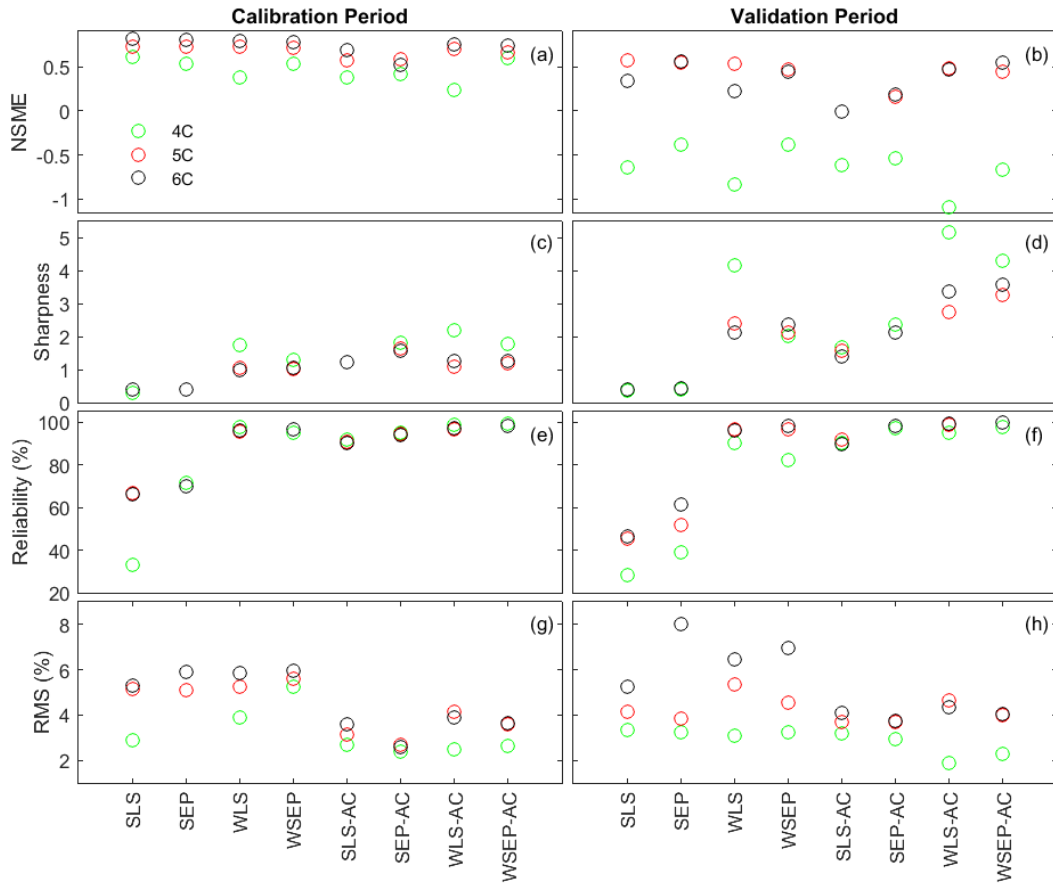
1071 Figure 8. Observation data (blue dots) and mean prediction (green line) and 95% credible intervals
 1072 (red line) of prediction ensembles for (a)-(f) the calibration period and (g)-(l) the validation period.
 1073 The plots are for the three soil respiration models using data models SLS and WSEP-AC. *The prediction ensembles are generated to consider parametric uncertainty of not only the soil*
 1074 *respiration models but also the data models.*
 1075
 1076



1077



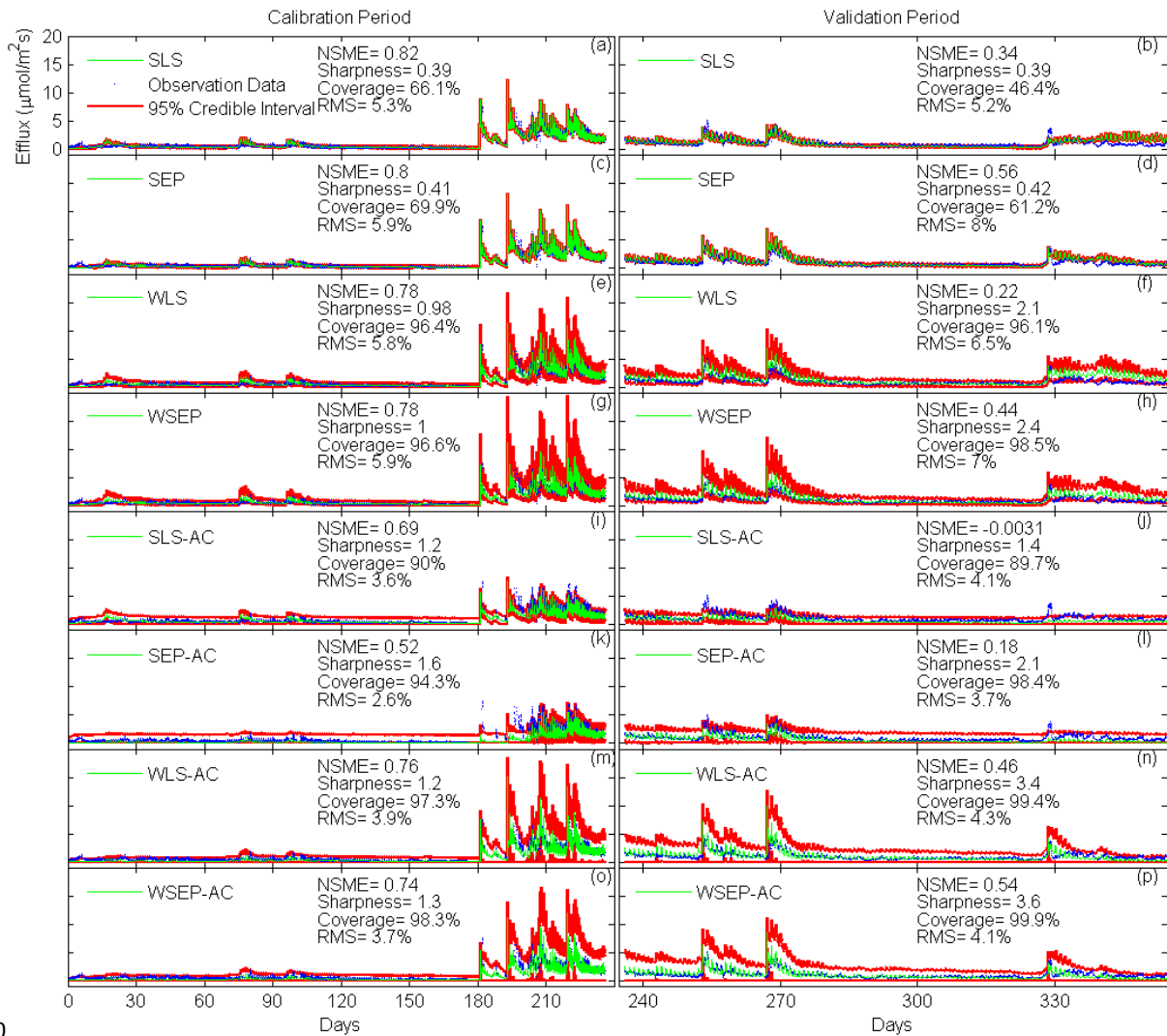
1078 Figure 9. (a-b) Nash-Sutcliffe model efficiency (NSME), (c)-(d) sharpness, (e)-(f) predictive
 1079 coverage, and (g)-(h) relative model score for measuring predictive performance of the three soil
 1080 respiration models and the eight data models during the calibration and cross-validation periods.
 1081 *The statistics are evaluated from the prediction ensembles generated to consider parametric*
 1082 *uncertainty of not only the soil respiration models but also the data models.*
 1083



1084



1085 Figure 10. Observation data (blue dots) and mean prediction (green line) and 95% credible
 1086 intervals (red line) for 6C for the eight likelihood functions during the calibration period (a)-(h)
 1087 and the validation period (i)-(p). *The prediction ensembles are generated to consider parametric*
 1088 *uncertainty of not only the soil respiration models but also the data models.*
 1089



1090